Review

Composite Forms in the System REE2O3 – ZrO2 – TiO2 for Minor Actinides (Am, Cm) and REEs Immobilization

Sergey V. Yudintsev , Michael I. Ojovan * , Olga I. Stefanovsky

Posted Date: 9 December 2024

doi: 10.20944/preprints202412.0652.v1

Keywords: spent nuclear fuel; reprocessing; high-level waste; rare earth elements – minor actinide fraction; immobilization; matrix; titanates; zirconates; properties; fabrication

 doi:10.20944/preprints202412.0652.v1

Review

Composite Forms in the System $REE_2O_3 – ZrO_2 – TiO_2$ for Minor Actinides (Am, Cm) and REEs Immobilization

Sergey V. Yudintsev [1], Michael I. Ojovan [1,2,*] and Olga I. Stefanovsky [3]

[1] Institute of Geology of Ore Deposits, Petrography, Mineralogy, and Geochemistry of the Russian Academy of Sciences, Staromonetny lane, 35, 119017 Moscow, Russia
[2] Immobilisation Science laboratory, School of Chemical, Materials and Biological Engineering, The University of Sheffield, Sheffield S1 3JD, UK
[3] A.N. Frumkin Institute of Physical Chemistry and Electrochemistry of the Russian Academy of Sciences, 119071 Moscow, Russia
* Correspondence: m.ojovan@sheffield.ac.uk

Abstract: The choice of efficient methods for immobilization of high-level waste (HLW) resulting from reprocessing of spent nuclear fuel (SNF) is an important scientific and practical task. The current policy of managing HLW within closed nuclear fuel cycle envisages its vitrification into borosilicate (B-Si) or alumina-phosphate (Al-P) glasses. These wasteforms have rather limited waste loading, and can potentially impair their retaining properties on devitrification. The optimal solution for HLW immobilisation could be by separating radionuclides into groups using dedicated capacious durable matrices. The phases of the $Nd_2O_3 – ZrO_2 – TiO_2$ system in this respect are promising hosts for REE – MA (MA = Am, Cm) fraction of HLW. We present herewith data on composition of samples analyzed, their durability in hot water, behavior under irradiation, and industrial manufacturing methods.

Keywords: spent nuclear fuel; reprocessing; high-level waste; rare earth elements – minor actinide fraction; immobilization; matrix; titanates; zirconates; properties; fabrication

1. Introduction

Over the past 65 years, the concentration of CO_2 in the Earth's atmosphere has increased by a quarter – from 315 ppm in 1958 to 420 ppm in 2023 and continues to grow. By March 2024, its level had increased by another 5 ppm, and this is the largest jump in the entire history of observations. A similar concentration of CO_2 in the air was reached 3-5 million years ago, when the temperature was higher by 2-3 °C, and the sea level was 10-20 meters higher than today. The increase in the amounts of climate-active gases is caused by the combustion of fossil fuels and transport. A huge contribution to environmental degradation is made by particulate matter, up to 2.5 micrometres in size, which causes up to 9 million premature deaths per year worldwide [1–3]. Low-carbon energy plays a key role in combating air pollution and global warming due to greenhouse gases [4,5]. Along with renewable sources, this also includes nuclear energy [6]. By 2026, the share of low-carbon generation in the world will reach 50%, with about a quarter of it coming from nuclear power plants [7]. The contribution of nuclear power to achieving carbon neutrality should increase by 2050, with the total capacity of nuclear power plants amounting to 890 GW(e) in the high and 458 GW(e) in the low scenario, compared to the current 369 GW(e), which is higher of former estimations [5]. Nuclear power is statistically the cleanest source of energy by the CO_2 emissions and the safest along with wind and solar power compared with coal, oil, gas, biomass and hydropower (Figure 1).

 doi:10.20944/preprints202412.0652.v1

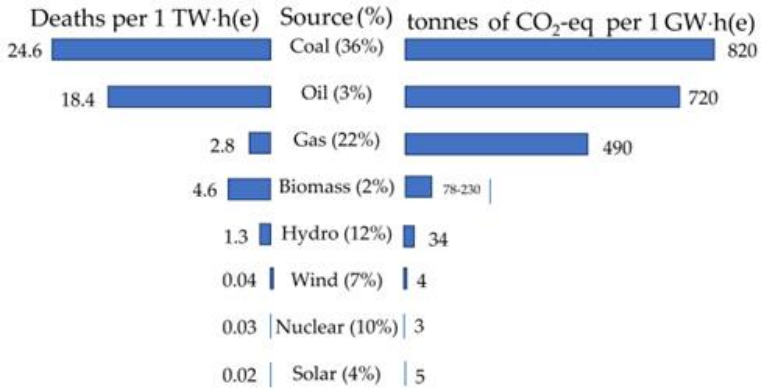

Figure 1. Characterization of energy sources by death rates caused by accidents, pollutions, and CO_2 emissions. Data on death rate are in events per 1 TW×h, and for CO_2 emissions are in tonnes per 1 GW×h of energy produced both of them during the lifecycle of operating power plants [8].

In November 2023, the European Parliament has categorized NE, along with 15 other technologies, as a "clean" technology. In December 2023, at the 28th UN Climate Conference (COP28, UAE), 22 countries, including the United States, Canada, United Kingdom, France, Japan, and South Korea, committed to triple the capacity of nuclear power plants by 2050 compared to 2020. It is expected that the share of nuclear generation in Russia will increase to 25% by 2045 from the current 20%. Investments in nuclear energy are growing worldwide; in many countries, they are either close to or have exceeded the costs of constructing hydrocarbon-fuelled power plants [9]. The implementation of these plans may be however hampered by a shortage of uranium and the problem of handling high-level waste (HLW). Based on the growth in the capacity of nuclear power plants and under the condition of an open fuel cycle with the disposal of spent nuclear fuel (SNF), their operation will require 2–3 times more uranium than nowadays: or 130–200 thousand tonnes per year. This threatens the rapid depletion of available natural uranium resources if the basis of nuclear energy in the future continues to be only thermal neutron reactors — light water reactors (LWR) [10]. These problems are solved by the transition to a two-component nuclear power system with thermal and fast neutron reactors with a closed nuclear fuel cycle - that is, the reprocessing of SNF, the separation of fission products, U and Pu from HLW, which are in demand for nuclear power generation, as well as minor actinides (Np, Am, Cm), which pose the greatest environmental hazard [11–15].

There are two ways of handling long-lived actinides and fission products [15,16]. The first is to separate them from HLW and then irradiate with neutrons for transmutation into stable or short-lived isotopes. However, its implementation encounters great technical difficulties and requires enormous costs [17]. The other method involves incorporating radionuclides into highly stable matrices and disposing them of [18–24]. In this case, the safety of HLW disposal facilities will be ensured by a bentonite-based sorption buffer, a corrosion-resistant container and robust HLW matrix. Additional barrier is the geological environment due to the low solubility of radionuclides in groundwater and their sorption by rocks around the disposal facility, and the slow flow of waters that carry radionuclides. In accordance with international standards [20] the preferred strategy for the management of radioactive waste is to contain it (i.e. to confine the radionuclides within the waste matrix, the packaging and the disposal facility) and to isolate it from the biosphere.

The current practice of isolating HLW involves its inclusion in borosilicate (B-Si) or alumina-phosphate (Al-P) glasses produced in electric furnaces or by induction melting [15,25–37]. The advantages of these glasses include a proven production technology and the ability to include many radioactive and stable isotopes. Their disadvantages include a low HLW load (5–20 wt.%), where the main part is made up of stable isotopes (REEs, Zr, Mo). The dry residue of liquid HLW from the reprocessing of LWR spent nuclear fuel contains up to 4 wt.% actinides and 50 wt.% fission products, most of which are stable [27,38]. In addition, the glasses can crystallize over time with the possible

 doi:10.20944/preprints202412.0652.v1

formation of more soluble phases, and when they come into contact with groundwater, colloids with high migration in the geological environment are formed.

Partitioning of HLW will allow actinides to be included in the most durable and thermodynamically stable crystalline matrices which might be components of integral composite systems containing both crystalline and vitreous wasteforms [25–28,37,39,40]. When selecting potential materials, phases with high loading in respect of the waste are firstly identified, then their corrosion and radiation resistance are studied, and finally the possibility of their remote industrial production is assessed.

We have considered possible crystalline matrices for immobilization of the REE – minor actinides (Am, Cm) fraction. By the size of the cation $(Am, Cm)^{3+}$ are close to Nd^{3+}, therefore the $Nd_2O_3 – ZrO_2 – TiO_2$ system is of interest, which contains $(Zr,Nd)O_{2-x}$ and $Nd_2(Zr,Ti)_2O_7$ with the fluorite or pyrochlore structure, $Nd_2Ti_2O_7$ of the perovskite type, as well as phases $Nd_4(Ti,Zr)_9O_{24}$ and Nd_2TiO_5, which have no natural structural analogues. This analysis was carried out based on literature data and the results of our own studies. The latter were mainly published in Russian journals and are little known to the world scientific community.

2. Separation of HLW for Groups of Radionuclides Isolation

The PUREX process (extraction of Pu and U) is the basis of SNF reprocessing; it can be supplemented by operations to extract other elements, including trivalent REE and minor actinides. The TRUEX, TODGA, and DIAMEX techniques allow for the extraction of REE, Am, and Cm; they have already been tested on real HLW [41–47]. Both the proportion of the REE-actinide fraction in SNF and the ratio of REE and actinides in it depend on the fuel composition, burnup, and storage time of SNF before reprocessing. The burnup of LWR reactor fuel reaches 45 GW×day per tonne; in the future, it is expected to be increased to 55 GW×day per tonne [42,48]. As the burnup increases from 30 to 45 GW×day, the REE content in a tonne of SNF increases from 10.2 to 13.9 kg, and the sum of Am and Cm – from 0.52 to 0.87 kg [41,49]. A tonne of SNF with a burnup of 60 GW×day contains 800 g Am (63% ^{241}Am, 37% ^{243}Am), 150 g Cm (90% ^{244}Cm, 8% ^{245}Cm, 1% each of ^{243}Cm and ^{246}Cm) and about 20 kg of REE. With an increase in SNF burnup to 70 GW×day, the Am content in a tonne of SNF will exceed 1 kg, and the amount of REE will be 23 kg (Table 1).

Table 1. The content of Am, Cm, REE in SNF (after 5 years of storage) and the proportion of Am and Cm in the mixture [50–52].

Element, g/t of SNF	Nuclear fuel burnup, GW × day per tonne of SNF						
	0.5	**20**	**33**	**40**	**51**	**60**	**70**
Σ Am	0.5	130	370	475	638	785	1080
Σ Cm	N.d.	N.d.	20	N.d.	78	135	N.d
Σ REE	220	7200	11200	~15000	n.d	~20000	~23000
(Am + Cm) : REE, %	0.2*	1.8*	3.4	3.1*	n.d.	4.4	4.5*

Note: N.d. – no data, * – excluding Curium.

During the storage of SNF, the composition of the REE-actinide fraction changes due to an increase in the proportion of ^{241}Am as a result of the decay of short-lived ^{241}Pu (half-life, $T_{½}$ = 14 years) and a decrease in the proportion of ^{244}Cm ($T_{½}$ = 18 years). An increase in the storage period of SNF from one year to 30 years increases the ratio $^{241}Am/^{243}Am$ from 1.3 to 12.1, and the proportion of actinides in the REE – MA mixture increases from 2% to almost 9% (Table 2).

Table 2. Am and Cm isotopes (g/t) in SNF with a burnup of 45 GW×day per tonne and the proportion of MA in the REE – MA mixture depending on the SNF storage time [52].

Radionuclide or mixture	After 1 year	After 5 years	After 30 years
^{241}Am	135	407	1272
^{243}Am	105	105	105

 doi:10.20944/preprints202412.0652.v1

Σ Am (ratio ^{241}Am / ^{243}Am)	240 (1.3)	512 (3.9)	1377 (12.1)
^{242}Cm	3.8	0.1	< 0.01
^{244}Cm	35.3	30.3	11.6
^{245}Cm	2.2	2.2	2.2
^{243,246,247,248}Cm	0.6	0.6	0.6
Σ total Cm	41.9	33.1	14.4
Σ MA (MA = Am и Cm)	281.9	545.1	1391.4
Cm / MA, %	14.9	6.1	1.0
MA / (REE* + MA), %	1.8	3.5	8.5

* A tonne of SNF with a burnup of 45 GW×day contains about 16 kg of rare earths.

Among the REE in SNF and HLW, the light elements of the cerium group with a large cation radius (from La to Sm) dominate, the content of which decreases in the sequence: Nd (about 39% of all REE) – Ce (23%) – La (12%) – Pr (10%) – Sm (8%) – Y (4%) and 4% Eu, Gd and Pm. Their isotopes are stable or have long half-lives and can be considered as stable, for example: ^{142}Ce (5.0×10^{16} years), ^{144}Nd (2.3×10^{15} years), ^{147}Sm (1.1×10^{11} years), ^{150}Nd (6.7×10^{18} years) [53]. Only a few isotopes have a short half-life: 285 days (^{144}Ce), 2.62 years (^{147}Pm), 4.76 (^{155}Eu), 8.6 (^{154}Eu) and 90 years (^{151}Sm). REE phases, especially Nd, are promising as matrices for the REE-actinide fraction, since it dominates among REE (40% of their total content) in SNF and HLW, and the radii of Nd^{3+} and REE-MA cations coincide and for coordination number (c. n.) VIII are equal to 1.09 Å [54]. Let us consider the Nd_2O_3 – ZrO_2 – TiO_2 system, first the edge parts, and then the entire three-component diagram.

ZrO_2 – TiO_2 System. There are oxides of the composition $(Ti,Zr)O_2$ (tetragonal structure of rutile), $(Zr,Ti)O_2$ (depending on the temperature, monoclinic – analogue mineral baddeleyite, or tetragonal) and $ZrTiO_4$ (analogue – mineral shrilankite) [55]. The content of REE in them is low and therefore they are not interesting as matrices for minor actinides. However, such phases are often found in experimentally obtained samples along with titanates and zirconates of REE. Further, for simplicity and convenience, we will use their abbreviated names: Z for ZrO_2, T in the case of TiO_2, ZT instead of $ZrTiO_4$ and so on.

Nd_2O_3 – ZrO_2 System. For the immobilisation of actinides, zirconate $Nd_2Zr_2O_7$, NZ with a pyrochlore structure and oxide $(Zr_{2-x}Nd_x)_2O_{2-0.5x}$ with a fluorite structure are promising, although it contains less REE-actinide fraction than pyrochlore (20 and 60 wt.%, respectively). The pyrochlore field is maximum at 1500 °C [56], and above 2200 °C it transforms into cubic oxide $(Zr_{2-x}Nd_x)_2O_{2-0.5x}$. These phases are also considered as inert matrix fuel for the transmutation of actinides, for example Am [16,57–59].

Nd_2O_3 – TiO_2 System. In this system, the greatest number of compounds – potential REE – MA hosts are formed: Nd_2TiO_5, $Nd_2Ti_2O_7$, $Nd_4Ti_9O_{24}$, $Nd_2Ti_3O_9$ [60]. Replacing Nd_2O_3 and TiO_2 with N and T, the phase formulas can be written as: NT (Nd_2TiO_5), NT_2 ($Nd_2Ti_2O_7$), N_2T_9 ($Nd_4Ti_9O_{24}$), NT_3 ($Nd_2Ti_3O_9$). The most important in this system (Table 3) are the eutectic of rutile and N_2T_9 (reaction No. 1), incongruent (No. 2) and congruent (No. 5) melting of the NT_2 and N_2T_9 phases. The NT_3 phase with a perovskite structure is formed at 1200 °C according to the reaction No. 4: $0.2\ N_2T_9 + 0.6\ NT_2 = NT_3$. Comparatively small differences in the structure of the Nd_2O_3–TiO_2 and La_2O_3–TiO_2 systems are observed (Table 3) [61,62], whereas in the Sm_2O_3–TiO_2 system, instead of the monoclinic phase, the $Sm_2Ti_2O_7$ compound with a cubic pyrochlore structure appears [63,64].

Table 3. Invariant points and phase reactions in the Nd_2O_3–TiO_2 and La_2O_3–TiO_2 systems [60,61].

№ п/п	Reaction scheme	T, K (°C)	Reaction scheme	T, K (°C)
1	$P \leftrightarrow T + N_2T_9$	1716 (1443)	$P \leftrightarrow T + L_2T_9$	1719 (1446)
2	$P + NT_3 \leftrightarrow N_2T_9$	1728 (1455)	$P + LT_3 \leftrightarrow L_2T_9$	1730 (1457)
3	$P + NT_2 \leftrightarrow NT_3$	1773 (1500)	$P + LT_2 \leftrightarrow LT_3$	1933 (1660)
4	$NT_3 \leftrightarrow N_2T_9 + NT_2$	1472 (1199)	$LT_3 \leftrightarrow L_2T_9 + LT_2$	1663 (1390)
5	$P \leftrightarrow NT_2$	2120 (1847)	$P \leftrightarrow LT_2$	2052 (1779)

 doi:10.20944/preprints202412.0652.v1

6	absent		$LT_2 + LT \leftrightarrow L_2T_3$	1873 (1600)
7	$P \leftrightarrow NT_2 + NT$	1973 (1700)	$P \leftrightarrow LT_2 + LT$	1958 (1685)
8	$P \leftrightarrow NT$	1993 (1720)	$P \leftrightarrow LT$	1983 (1710)
9	$P \leftrightarrow N + NT$	1774 (1501)	$P \leftrightarrow L + LT$	1719 (1446)

P – molten product, T – TiO_2, N_2T_9 – $Nd_4Ti_9O_{24}$, NT_3 – $Nd_2Ti_3O_9$, NT_2 – $Nd_2Ti_2O_7$, NT – Nd_2TiO_5, N – Nd_2O_3, L_2T_9 – $La_4Ti_9O_{24}$, LT_3 – $La_2Ti_3O_9$, LT_2 – $La_2Ti_2O_7$, LT – La_2TiO_5, L_2T_3 – $La_4Ti_3O_{12}$, L – La_2O_3.

The $REE_2Zr_2O_7$ and $REE_2Ti_2O_7$ phases (REE = La, Nd) crystallize in a cubic (pyrochlore) or monoclinic (perovskite type) structure [65–68]. Pyrochlore is formed when the ratio of the radii of REE^{3+} and $(Ti,Zr)^{4+}$ is in the range from 1.46 to 1.78 Å; in other cases, the fluorite structure of REE zirconates and the perovskite structure of titanates are stable. The $REE_2Ti_2O_7$ (Sm–Yb, Y) and $REE_2Zr_2O_7$ (La–Gd) phases have a pyrochlore structure. Depending on the REE type, the REE2TiO5 phases have an orthorhombic (La–Sm), cubic (Er–Lu, Sc) or hexagonal (Eu–Ho, Y) structure [69]. These features have a significant impact on the capacity of the phases with respect to the actinide components of the HLW.

3. Crystal – Chemical Features of Rare Earth Zirconates and Titanates

The content of REE and actinides is one of the important criteria for selecting a matrix for immobilization of the radionuclides of REE – MA fraction. Crystal chemistry and structural features of the phases formed in the REE_2O_3 – ZrO_2 – TiO_2 system were considered using the example of Nd^{3+} [70] and are briefly discussed below.

$Nd_2Zr_2O_7$ Phase has a cubic lattice (Figure 2a), space group *Fd-3m*. There are 8 formula units in the unit cell, the Nd polyhedron is a scalenohedron (distorted cube), contains 8 O atoms - six equidistant from Nd^{3+} and two at a greater distance. Zr cations are surrounded by six O atoms at the vertices of a trigonal antiprism (distorted octahedron). The structure of pyrochlore can be also described through interpenetrating frameworks of BO_6 and A_2X octahedra, it is derived from a fluorite-type lattice (space group *Fm-3m*).

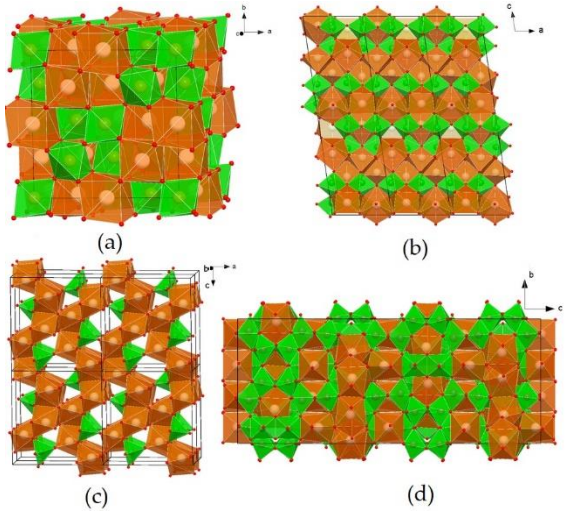

Figure 2. Structures of the phases $Nd_2Zr_2O_7$ (a), $Nd_2Ti_2O_7$ (b), Nd_2TiO_5 (c), and $Nd_4Ti_9O_{24}$ (d). Green – Ti and Zr polyhedra, brown – Nd polyhedra, red circles – atoms of Oxygen.

The structure $Nd_2Ti_2O_7$ is derived from the perovskite-type structure (Figure 2b): TiO_6 octahedra, connecting at their vertices, form plates of 4 octahedra (about 12 Å) in the *a* and *b* directions, between which single-capped trigonal prisms of NdO_7 are located. Three-capped trigonal prisms of NdO_9 fill the cavities of the octahedral blocks. Two-capped prisms of NdO_8 are located inside and between the octahedral blocks. The structure of $Nd_2Ti_2O_5$ (Figure 2c) consists of edge-linked seven-vertex NdO_7 and chains of square pyramids of TiO_5, connected by vertices in the [010] direction. The most complex structure of $Nd_4Ti_9O_{24}$ is represented by a titanium-oxygen framework, and Nd polyhedra are located

 doi:10.20944/preprints202412.0652.v1

in its cavities (Figure 2d). Nd atoms occupy 3 positions: Nd(1) polyhedron – distorted square antiprism, Nd(2) – octahedron, Nd(3) – distorted square prism. The Nd(1)O_8 polyhedra, connecting by edges and vertices, form layers parallel to the (110) plane. The Nd(3) polyhedra are connected by edges with Nd(1) layers and form 17.5 Å thick blocks, in the channels of which Nd(2) octahedra are located.

The REE^{3+} cations are characterized by coordination numbers (c. n.) equal to VII (one-capped trigonal prism, truncated cube), VIII (cube, two-capped antiprism) and IX (three-capped trigonal prism). The coordination polyhedra of the smaller Zr^{4+} and Ti^{4+} cations have the shape of an octahedron (c.n. = VI), except for Nd_2TiO_5, c. n. of Ti^{4+} = V, and this polyhedron is a square pyramid. The low "solubility" of impurities corresponds to odd c. n. (VII and IX) in Nd–O polyhedra, and high solubility corresponds to even c. n. (VIII). This explains the wide field of the pyrochlore solid solution and the narrow composition fields of the remaining phases. Pyrochlore $Nd_2(Zr,Ti)_2O_7$ has a high capacity of the structure with respect to actinides: up to 20 at.% U enters the Zr^{4+} position, and from 10 to 20 at.% U and Th enter the Nd^{3+} position. Some of the Nd^{3+} ions in $Nd_4Ti_9O_{24}$ have c. n. = VIII, which is probably resulted in a higher content of impurities (Ca, U and Zr) in this phase compared to $Nd_2Ti_2O_7$ and Nd_2TiO_5 [70–74].

Phase diagrams of systems REE_2O_3–ZrO_2–TiO_2 depend on the REE^{3+} radius (Figure 3).

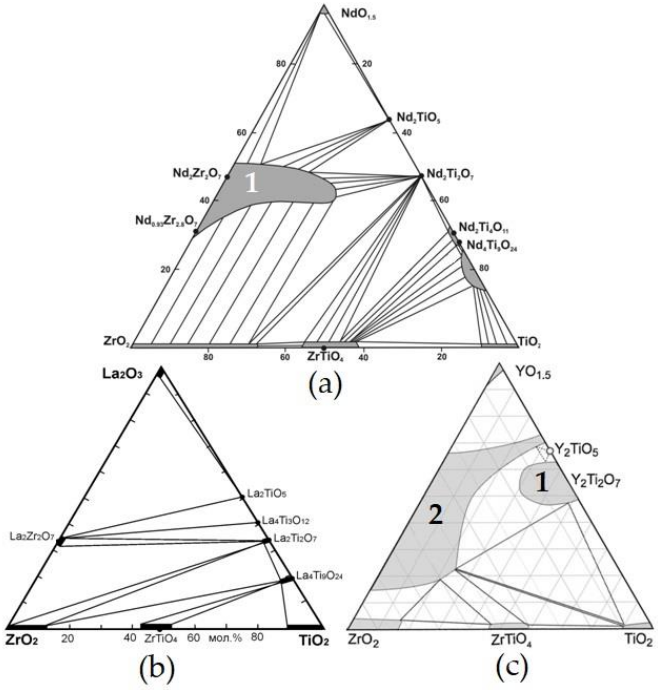

Figure 3. Systems $NdO_{1.5}$–TiO_2–ZrO_2 (a), La_2O_3–TiO_2–ZrO_2 (b) and $YO_{1.5}$–TiO_2–ZrO_2 (c) at 1350 °C – 1500 °C. Fields of pyrochlore (1) and oxide with a fluorite structure (2) are shown [65,74–76].

Replacement of Nd^{3+} by La^{3+} has a weak effect, whereas a decrease in the ionic radius from Nd^{3+} to Sm^{3+}, Gd^{3+} and Y^{3+} leads to a more significant change [74–77]. The La_2O_3–TiO_2–ZrO_2 system also contains: La_2TiO_5 (LT), $La_4Ti_3O_{12}$ (L_2T_3), $La_2Ti_2O_7$ (LT_2), $La_4Ti_9O_{24}$ (L_2T_9), $La_2Zr_2O_7$ (LZ_2), $ZrTiO_4$ (ZT), ZrO_2 (Z), TiO_2 (T). Systems with Nd_2O_3 and La_2O_3 are similar in the set of phases, however, in the system with lanthanum, the pyrochlore region is smaller. When large ions La^{3+} and Nd^{3+} are replaced by Y^{3+}, $Y_2Ti_2O_7$ (pyrochlore) is formed and a cubic oxide $(Zr,Y)O_{2-x}$ with a fluorite structure appears. The structure of Y_2TiO_5 is cubic (sp. group *Fm-3m*), but Nd_2TiO_5 and La_2TiO_5 have orthorhombic symmetry (sp. group *Pnma*). A feature of Nd and La titanates is slight variations in composition, the Ti : REE ratios in them are close to the values in the formulas (Figure 3). At 1350 °C, the LT_2, L_2T_3 and LT phases contain less than 2 mol.% ZrO_2, the ZrO_2 content in L_2T_9 is higher and equals 4 mol.%, the content of La_2O_3 and ZrO_2 in $La_2Zr_2O_7$ reaches 35 mol.% and 69 mol.% (Table 4). The isomorphism of La^{3+} in ZrO_2 and $ZrTiO_4$ is limited to 1 mol.% La_2O_3. In $(Ti,Zr)O_2$ and $(Zr,Ti)O_2$, high contents of ZrO_2 and TiO_2 (12–14 mol.%) are found, Zr:Ti ratio in $ZrTiO_4$ varies from 1.4 to 0.9.

 doi:10.20944/preprints202412.0652.v1

Table 4. Variations in the phase composition (mol.%) in the La_2O_3 – TiO_2 – ZrO_2 system [75].

Phase and its designation	La_2O_3	TiO_2	ZrO_2
$La_2Ti_2O_7$, LT_2	32.3 ± 0.3	66.2 ± 0.2	1.5 ± 0.3
	31.7 ± 0.9	67.2 ± 1.0	1.1 + 0.2
$La_4Ti_9O_{24}$, L_2T_9	17.7 ± 1.0	81.1 ± 1.1	2.2 + 0.3
	16.7 ± 0.5	78.9 ± 0.6	4.4 ± 0.2
$ZrTiO_4$, ZT	< d.l.	53.1 ± 0.4	46.9 ± 0.3
	< d.l.	41.6 ± 0.3	58.4 ± 0.3
ZrO_2, Z_t	< d.l.	13.5 ± 0.6	86.5 ± 0.7
TiO_2, T	< d.l.	88.6 ± 0.5	11.4 ± 0.3

< d.l. – less than the detection limit of the SEM/EDS method, equal to 0.3–0.5 wt.%.

4. Actinide Waste Forms in the REE_2O_3 (Nd_2O_3) – ZrO_2 – TiO_2 System

Let us consider the issue of matrices for the REE – actinide fraction in the REE_2O_3 (Nd_2O_3) – ZrO_2 – TiO_2 system taking into account the data [65,78] and previous our results [62,70–74,79–82]. About 30 samples were synthesized by cold pressing and sintering (CPS) of the oxide mixture at 1400–1550 °C or by induction cold crucible melting (ICCM). The samples were analysed on a Rigaku D/Max 2200 X-ray diffractometer (XRD, Cu Kα) and in a JSM–5610LV scanning electron microscope with a JED–2300 energy-dispersive spectrometer (SEM/EDS). To determine corrosion resistance, their interaction with water and brines was studied at 90–240°C for 30–143 days. After the tests, the solutions were analysed for REE content; to determine the colloidal form, they were filtered through membranes with pore sizes of 450, 200, 100, and 25 nm. The compositions of the solution and its filtrates were analysed using inductively coupled plasma mass spectrometer (XII ICP-MS Thermo Scientific). The samples were irradiated with 1 MeV Kr^{2+} (flux density of 10^{12} ions /cm^2×s) on an accelerator at the Argonne National Laboratory in the USA at T = 50–1023 K. Some of the samples were irradiated with 4.5–5 MeV electrons at JSC SRC "RIAR" (Russia) with subsequent study of their structure and hydrolytic stability.

As before, we will use mineral names or designations for the phases based on their formulas, where Nd_2O_3, ZrO_2 and TiO_2 are replaced by N, Z and T. In the Nd_2O_3–TiO_2–ZrO_2 system there are [65,78] phases $Nd_2(Ti,Zr)_2O_7$ (NTZ) with a pyrochlore structure, TiO_2 (T), $ZrTiO_4$ (ZT) and tetragonal ZrO_2 (Z). Nd titanates are represented by: Nd_2TiO_5 (NT), $Nd_2Ti_2O_7$ (NT_2), $Nd_2Ti_4O_{11}$ (NT_4), $Nd_4Ti_9O_{24}$ (N_2T_9). In [60], the identity of $Nd_2Ti_4O_{11}$ and $Nd_4Ti_9O_{24}$ was proven and the phase $Nd_2Ti_3O_9$ (NT_3) was found. The largest field in the Nd_2O_3–ZrO_2–TiO_2 diagram is occupied by pyrochlore, smaller variations in composition are characteristic of $Nd_4Ti_9O_2$ (Figure 3a), which makes these phases promising hosts for the REE-actinide fraction. Below, data on samples prepared by CPS or ICCM routes composed of the pyrochlore or orthorhombic REE titanate are discussed.

4.1. Samples of the Composition $(REE)_2(Zr,Ti)_2O_7$ with a Pyrochlore Structure

To check the pyrochlore region boundaries, samples whose composition points lie on the $REE_2Zr_2O_7$ – $REE_2Ti_2O_7$ line (Figure 4) were studied. They were obtained by sintering for 5 h at 1400 °C (Zr : Ti ≤ 1) or 1550 °C (Zr : Ti > 1). The batch charge was prepared from TiO_2, ZrO_2 and REE_2O_3 in quantities corresponding to the formula $REE_2Zr_{2-x}Ti_xO_7$, "x" varies from 0 (sample T0) to 2 (T20) with a step of 0.1 or 0.2. The proportions of REE oxides corresponded to the contents in the SNF and were, in wt% as follows: 11.8 La_2O_3, 23.0 Ce_2O_3, 10.7 Pr_2O_3, 38.9 Nd_2O_3, 8.1 Sm_2O_3, 1.3 Eu_2O_3, 1.5 Gd_2O_3, 4.7 Y_2O_3. Up to x = 0.8 (T0 – T8), the samples consist of pyrochlore; at a higher titanium content, monoclinic REE titanate with a perovskite structure appears. This phase becomes the main one at x > 1.2, i.e. in samples T12 – T20. The content of total REE oxides in it is approximately 10 % higher than in pyrochlore – 65 and 55 wt%, respectively (Table 5).

Preprints.org (www.preprints.org) | NOT PEER-REVIEWED | Posted: 9 December 2024 doi:10.20944/preprints202412.0652.v1

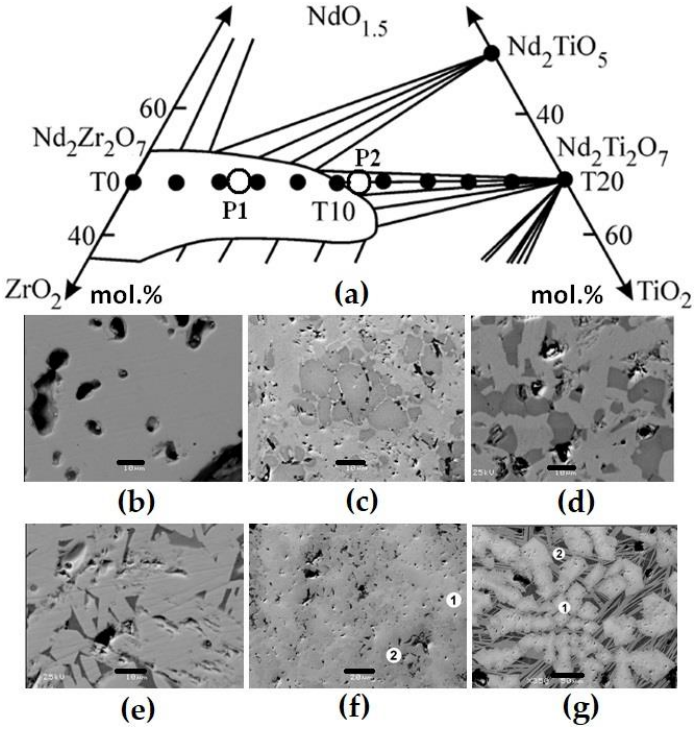

Figure 4. Part of the $NdO_{1.5}$–ZrO_2–TiO_2 diagram (a) and the compositions of ceramics obtained by sintering (T0–T20, dark circles) or melting (rings), and SEM images of samples T0 (b), T15 (c), T18 (d), T20 (e), P1 (f), and P2 (g). Light – pyrochlore, dark – REE titanate. According to [71,81]. Scale bars are 10 (b – e), 20 (f) and 50 (g) microns.

Table 5. Compositions (wt%) and formulas of the pyrochlore (p) and monoclinic phases (m).

№	TiO_2	ZrO_2	Y_2O_3	La_2O_3	Ce_2O_3	Pr_2O_3	Nd_2O_3	Sm_2O_3	Eu_2O_3	Gd_2O_3
T0 (p)	0	45.7	2.6	7.5	12.6	5.1	19.2	3.7	1.7	1.9
	$(Y_{0.12}La_{0.25}Ce_{0.41}Pr_{0.17}Nd_{0.62}Sm_{0.11}Eu_{0.05}Gd_{0.06})Zr_{2.0}O_{6.69}$									
T15 (p)	19.8	23.7	5.8	4.2	12.6	5.1	20.3	5.4	1.2	1.9
	$(Y_{0.23}La_{0.12}Ce_{0.35}Pr_{0.14}Nd_{0.55}Sm_{0.14}Eu_{0.03}Gd_{0.05})(Ti_{1.21}Zr_{0.79})O_{6.42}$									
T15 (m)	33.0	1.6	2.4	11.6	16.2	6.5	23.3	3.8	0.7	0.9
	$(Y_{0.10}La_{0.33}Ce_{0.46}Pr_{0.19}Nd_{0.65}Sm_{0.10}Eu_{0.02}Gd_{0.02})(Ti_{1.94}Zr_{0.06})O_{6.82}$									
T18 (m)	33.1	0.7	2.2	10.4	17.0	6.4	23.6	4.2	1.1	1.3
	$(Y_{0.09}La_{0.31}Ce_{0.50}Pr_{0.19}Nd_{0.67}Sm_{0.12}Eu_{0.03}Gd_{0.03})(Ti_{1.97}Zr_{0.03})O_{6.89}$									
T20 (m)	33.4	0	2.9	8.9	16.0	6.0	25.1	5.2	1.4	1.2
	$(Y_{0.12}La_{0.26}Ce_{0.47}Pr_{0.17}Nd_{0.71}Sm_{0.14}Eu_{0.04}Gd_{0.03})Ti_{2.0}O_{6.92}$									

Samples P1 and P2 (Figure 4) were obtained by the induction cold crucible melting (ICCM) method; neodymium (P1) or a mixture of lanthanum, cerium and gadolinium (P2) were waste simulants. The synthesis was carried out in air; a zirconium ring was placed in the batch for melting. After the melt was formed and the batch was loaded, it was melted for 0.5 h, then the setup was turned off for cooling and forming a ceramic block. The composition of sample P1 (formula $Nd_2Zr_{1.5}Ti_{0.5}O_7$) lies in the pyrochlore field (Figure 4). According to XRD and SEM/EDS data, it is composed of pyrochlore, the composition of which varies within the sample (Table 6). Light areas are enriched in Zr (on average 41.5% ZrO_2) compared to dark ones (36.6%), the Nd_2O_3 contents are similar.

Table 6. Phase compositions (wt%) and atomic quantities of elements based on 7 O^{2-}.

 doi:10.20944/preprints202412.0652.v1

Oxide / cation	Sample P1: Pyrochlore, light – dark	Sample P2: Pyrochlore, centre – edge (average)	Sample P2: Monoclinic REE titanate
TiO_2	3.7 – 8.4	4.6 – 14.1 (9.1)	31.8
ZrO_2	41.5 – 36.6	36.1 – 23.2 (30.0)	No
La_2O_3	No	6.9 – 11.6 (10.2)	25.5
Nd_2O_3	54.8 – 55.0	No	No
Ce_2O_3	No	11.9 – 12.4 (11.7)	17.1
Gd_2O_3	No	38.2 – 35.5 (37.8)	23.9
Ti^{4+}	0.26 – 0.57	0.34 – 0.99 (0.65)	2.01
Zr^{4+}	1.88 – 1.61	1.72 – 1.06 (1.39)	No
La^{3+}	No	0.25 – 0.40 (0.36)	0.79
Nd^{3+}	1.82 – 1.77	No	No
Ce^{3+}	No	0.43 – 0.43 (0.41)	0.53
Gd^{3+}	No	1.24 – 1.10 (1.19)	0.67

The composition of sample P2, wt.% is 14.6 TiO_2, 22.4 ZrO_2, 14.9 La_2O_3, 15.0 Ce_2O_3, 33.1 Gd_2O_3, formula $(La_{0.5}Ce_{0.5}Gd)TiZrO_7$ and is located at the edge of the pyrochlore field. Pyrochlore dominates in it (85–90%), REE titanate is present (Figure 4). From the centre to the edges of the pyrochlore grains, the concentration of zirconium and lanthanum decreases (Table 6), and that of gadolinium and titanium increases. Pyrochlore is enriched in ZrO_2 and Gd_2O_3 but contains less La_2O_3 and Ce_2O_3 relative to REE titanate. REE titanate is located between the pyrochlore grains, which indicates its late formation. Another phase of the composition, wt.%: 18.7 TiO_2, 5.1 ZrO_2, 26.7 La_2O_3, 15.0 Ce_2O_3, 13.5 Gd_2O_3, 18.6 SiO_2, 2.4 Fe_2O_3 by the ratio of REE: (Ti + Zr + Fe) : Si is close to the mineral perrierite $(La,Ce)_2Ti_2Si_2O_{11}$. It is formed due to the dissolution of the crucible coating, which explains the localization in the marginal parts and the presence of Si and Fe.

4.2. Samples of the Composition $(REE)_2(Zr,Ti)_2O_7$ with a Pyrochlore Structure

Samples with the $(REE)_4Ti_9O_{24}$ phase containing 48 wt.% of the REE-actinide fraction were obtained by sintering or melting–crystallization. The points of the bulk compositions of the samples lie near or in the field of this phase at the Figure 3a. Sample RT-1 (Figure 5, Table 7) composed of REE titanate (light) and titanium oxide with a rutile structure (dark), was obtained by sintering for 4 h at 1375 °C of a mixture, wt.%: 52 TiO_2, 45 Nd_2O_3, 3 Sm_2O_3 (formula $Nd_{3.75}Sm_{0.25}Ti_9O_{24}$). Several samples (IM-1, IM-2, RT-2, MPM-1) were obtained by the ICCM method at 1500 °C. They are composed of orthorhombic titanate and rutile, the proportion of which depends on the composition of the batch and varies from 10 to 50% (Figure 5). Rutile contains 3–8 wt.% ZrO_2, where Zr^{4+} replaces Ti^{4+} due to close radii (0.72 Å and 0.61 Å). The formula of REE titanate is calculated for 24 O^{2-}, the sum of Ti^{4+} and Zr^{4+} is close to 13 (Table 7). It contains up to 3 wt.% ZrO_2. Analysis of the samples in a high-resolution electron microscope (Figure 5f) confirmed the orthorhombic symmetry (sp. Gr. *Fddd*) and the unit cell parameters, Å: "a" = 14.0, "*b*" = 35.5, "*c*" = 14.6.

 doi:10.20944/preprints202412.0652.v1

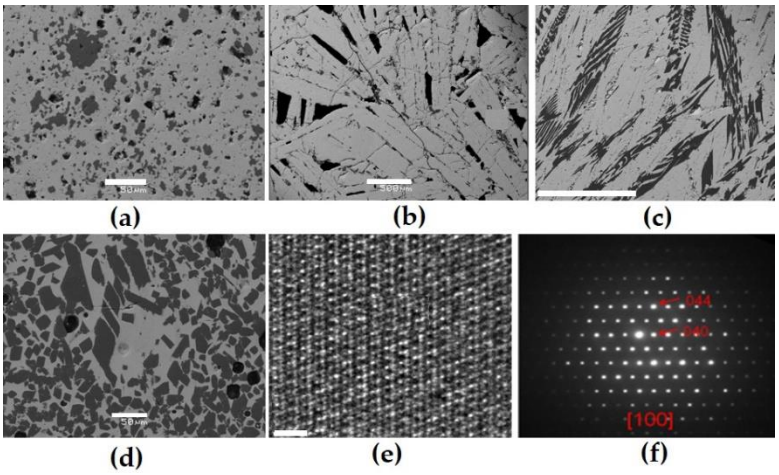

Figure 5. SEM images of samples obtained by sintering: RT-1 (a) or melting: IM-9 (b), RT-2 (c), MLM-1 (d) and electron diffraction patterns for orthorhombic rare-earth titanate in the MLM-1 sample (e, f). 1 – orthorhombic rare-earth titanate (light), 2 – rutile (dark). Scale bars are 50 (a, d) and 500 (b, c) microns or 2 nm (e).

Table 7. Compositions (wt.%) and formulas of the rare earth titanate (dash – element not entered).

Sample	TiO_2	ZrO_2	Y_2O_3	La_2O_3	Ce_2O_3	Pr_2O_3	Nd_2O_3	Sm_2O_3	Eu_2O_3	Gd_2O_3
RT-1	51.8	-	-	-	-	-	44.9	3.3	-	-
	$Nd_{3.72}Sm_{0.26}Ti_9O_{24}$									
IM-9	51.2	1.0	-	-	-	-	47.8			
	$Nd_{3.94}(Ti_{8.88}\ Zr_{0.12})O_{23.91}$									
RT-2	51.1	1.4	-	-	-	-	47.5	-	-	-
	$Nd_{3.95}(Ti_{8.86}Zr_{0.16})O_{24}$									
MLM-1	51.5	2.9	1.4	5.2	11.4	3.1	20.1	2.4	1.1	0.9
	$(Y_{0.17}La_{0.44}Ce_{0.95}Pr_{0.26}Nd_{1.63}Sm_{0.19}Eu_{0.09}Gd_{0.07})(Ti_{8.83}Zr_{0.32})O_{24}$									
IM-2	50.5	3.0	1.9	4.9	10.9	3.5	19.8	3.1	1.2	1.2
	$(Y_{0.23}La_{0.42}Ce_{0.92}Pr_{0.30}Nd_{1.63}Sm_{0.25}Eu_{0.10}Gd_{0.09})(Ti_{8.71}Zr_{0.34})O_{24}$									

Samples obtained via melting have larger grain sizes than those obtained by sintering. The melting temperatures of samples with orthorhombic titanate are about 1500 °C. This is 100–250 °C lower than that of Ti-Zr pyrochlore, which simplifies the synthesis.

5. On the Pseudo-Ternary Nature of the Nd_2O_3 – ZrO_2 – TiO_2 System

The Nd_2O_3 – ZrO_2 – TiO_2 system was previously considered as ternary, however, in the case of partial reduction of Ti^{4+} (TiO_2) to Ti^{3+} (Ti_2O_3), it becomes quaternary. A sample of the composition, mol.%: 21 Nd_2O_3, 16 ZrO_2 and 63 TiO_2 was synthesized by melting in a glass-carbon crucible [82]. According to the data [65,78], it should consist of $Nd_2Ti_2O_7$ and $ZrTiO_4$, however, according to the results of X-ray diffraction and SEM/EDS studies, the sample is composed of two Nd titano-zirconates of different colours and compositions (Figure 6, Table 8) and rutile. Electron back scatter diffraction (EBSD) confirmed the structure of pyrochlore for the light phase and zirconolite for the dark one (Figure 6). When the melt interacts with glass-carbon crucible, the reaction occurs: $2Ti^{4+}O_2 + C = Ti^{3+}{}_2O_3 + CO$. Ti^{3+} ions serve as charge compensators during the exchange: $Nd^{3+} + Ti^{3+} \rightarrow Ca^{2+} + Ti^{4+}$, which leads to the formation of zirconolite (ideally $CaZrTi_2O_7$), in which Ca^{2+} is fully replaced by Nd^{3+}. Based on the composition of the phases (Table 8), their formulas were calculated with Ti^{4+} only and taking into account Ti^{3+}. Reducing conditions are necessary for Ti^{3+} appearance, but only Ti^{4+} is stable at the synthesis in air, and the system is ternary.

Preprints.org (www.preprints.org) | NOT PEER-REVIEWED | Posted: 9 December 2024 doi:10.20944/preprints202412.0652.v1

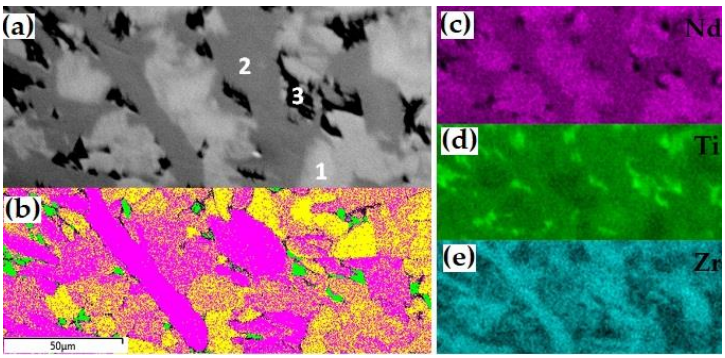

Figure 6. SEM image (a: 1 – pyrochlore, 2 – zirconolite, 3 – rutile), EBSD map (b: yellow – pyrochlore, purple – zirconolite, green – rutile) and distribution of Nd (c), Ti (d) and Zr (e) in sample with Ti^{3+}.

Table 8. Compositions (wt.%) and phases formulae, for zirconolite the option with Ti^{3+} is shown.

Phase		Ti	Zr	Nd	O	Only Ti^{4+}	With Ti^{3+} also
Pyrochlore		16.5	13.1	46.9	23.5	$Nd_{1.35}Zr_{0.59}Ti_{1.41}O_{6.02}$	$Nd_{1.35}Zr_{0.59}Ti_{1.41}O_{6.02}$
Zirco-	centre	21.5	14.6	38.1	25.8	$Nd_{1.22}Zr_{0.74}Ti_{2.04}O_{7.4}$	$Nd_{1.22}Zr_{0.74}Ti^{4+}_{1.26}Ti^{3+}_{0.78}O_7$
nolite	edge	23.5	11.8	38.5	26.2	$Nd_{1.20}Zr_{0.60}Ti_{2.20}O_{7.4}$	$Nd_{1.20}Zr_{0.60}Ti^{4+}_{1.40}Ti^{3+}_{0.80}O_7$
Rutile		46.8	7.0	10.7	35.5	$Ti_{0.86}Zr_{0.07}Nd_{0.07}O_{1.97}$	$Ti_{0.86}Zr_{0.07}Nd_{0.07}O_{1.97}$

6. Behavior of the Matrices with REE – Actinide Fraction in Hot Aqueous Solutions

Along with the waste capacity, a very important characteristic of actinide matrices is their resistance to leaching. A number of standard tests have been developed to determine this parameter [25,26,28,36,39,83]. The behaviour of pyrochlore has been studied in static and dynamic tests [64,66,68,73,84–87]. The normalized leaching rate of U and REE from titanate pyrochlore under near-neutral conditions is 10^{-4} – 10^{-5} g/(m² × day), it increases by an order of magnitude in alkaline (pH > 9) or acidic solutions (pH < 5). This is 3 orders of magnitude lower than leaching from HLW glass matrices under similar conditions [88,89]. The rates of actinide and REE leaching from zirconate pyrochlores are lower than from titanate ones. For pyrochlore $La_2Zr_2O_7$ in static tests in water and alkaline solution (pH = 10) at 90–150 °C, the values for La are below 10^{-4} g/m² day, and for Zr are equal to 10^{-6} g/(m² × day) [90–92]. The rate of plutonium leaching from titanate pyrochlores before their amorphization (MCC-1, water, 90 °C, 14-28 days) varies from ~10^{-2} to 10^{-4} g/(m² × day). The spread of values is probably due to the presence of other phases in the samples, in addition to pyrochlore. After amorphization, the rate of Pu leaching increases to 7×10^{-2} – 9×10^{-3} g/(m² × day). Leaching of Cm from pyrochlore $(Gd,Cm)_2Ti_2O_7$ after amorphization increased from 10^{-2} to 2×10^{-1} g/(m² × day) [89,93,94]. For pyrochlore $(Gd,Cm)_2(TiZr)O_7$ the values of 1.7×10^{-2} and 4.7×10^{-2} g/(m² × day) were obtained [94]. Amorphization increases the rate of actinide leaching by 3–10, rarely 50 times [66,87,89,93–97]. Therefore, in runs with short-lived actinides (^{244}Cm), rate of actinide leaching increases due to phase amorphization, as well as an increase in the acidity of the solution to pH = 4 due to its radiolysis.

Studies of the corrosion resistance of the $REE_2Ti_2O_7$ and $REE_4Ti_9O_{24}$ phases are rare [64,73,79,80,98,99]. The leaching rates of La and Nd (95–240 °C, water, brine, 30–143 days) are close to the values for pyrochlore and vary from 10^{-3} to 10^{-5} g/(m² × day), which corresponds to the dissolution of a matrix layer a few microns thick in a year. Taking into account the studies [66,72,73,80], we conclude that pyrochlore and Nd titanates are resistant to corrosion in hot waters. Incongruent dissolution with a higher leaching rate of REE and actinides compared to Ti and Zr is typical for them. This leads to the formation of a surface layer, tens of nm thick, enriched with these elements, which complicates leaching of actinides [64,92,96]. After 40 days of contact of the pyrochlore with a solution of 0.5 M $CaCl_2$ + 0.5 M NaCl (T = 200 °C), no changes were detected in the SEM (Figure 7).

 doi:10.20944/preprints202412.0652.v1

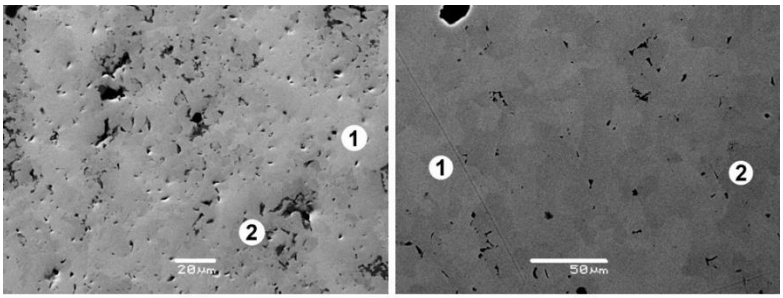

Figure 7. Images of sample P1 before (a) and after contact with brine (b) 1, 2 – pyrochlore grains of different color and composition (Table 6). From [73].

7. Behavior of the Matrices with REE – Actinide Fraction Under Irradiation

The sources of radiation in the HLW forms are β- and α-decay, γ-radiation, spontaneous fission of actinides (Tables 9 and 10). The disordering of the crystalline structure is mainly due to the formation of α-particles and heavy recoil nuclei during actinide decay. α-particles (He^{2+} with an energy of 4.5–5.5 MeV) account for up to 98% of the decay energy. At the end of a range of 10–20 μm, they collide with hundreds of atoms, knocking them out of their original position (Table 10). Recoil nuclei with an energy of 70–100 keV collide with 1–2 thousand atoms on a path of 10–40 nm. The role of beta particles, gamma radiation, and neutrons in this aspect is small. Influence of spontaneous fission of heavy actinides increases starting from ^{244}Cm, but this effect is weak due to their low content.

Table 9. Composition and properties of a mixture of Am and Cm isotopes isolated from a tonne of SNF of a PWR-type reactor with a burnup of 50 GW×day after 6 years of storage [100].

Nuclide ($T_{1/2}$, years)	Share, wt.%	Heat release, W/kg	Decay and its probability	Emission, particles/s		Daughter nuclide $T_{1/2}$, years
				α-particles	neutrons	
^{241}Am (433)	63.85	114.7	α + SF (3.8×10^{-12})	1.3×10^{11}	2752	^{237}Np (2.1×10^{6})
^{243}Am* (7.3×10^{3})	25.35	6.4	α + SF (3.7×10^{-11})	7.4×10^{9}	139	^{239}Pu (2.4×10^{4})
^{243}Cm (29.1)	0.09	1860.7	α (0.9976) + β^+ (0.0024)	1.9×10^{12}	48690	^{239}Pu (2.4×10^{4})
^{244}Cm (18.1)	9.78	2841.8	α + SF (1.4×10^{-6})	3.0×10^{12}	10.9×10^{6}	^{240}Pu (6537)
^{245}Cm (8.5×10^{3})	0.82	5.8	α (1.0)	6.4×10^{9}	123	^{241}Pu (14.4)
^{246}Cm (4.76×10^{3})	0.11	10.2	α + SF (2.6×10^{-4})	1.1×10^{10}	8.76×10^{6}	^{242}Pu (3.8×10^{5})

The content of isotopes ^{242}Am and ^{242}Cm is less than 0.01 wt.%. * – ^{239}Np is formed ($T_{1/2}$ = 2.36 days), which is converted into ^{239}Pu. α – alpha decay, SF – spontaneous fission, β^+ – positron decay. A tonne of SNF contains about 17 kg of REE and 0.7 kg of MA (Am and Cm).

Table 10. Radiation effects in solidified forms of HLW according to data from [25,50,93,95,97,101].

Type of radiation (decay)	Range of defects, m	Irradiation dose, Gray* after 10^4 / 10^6 years	Atomic displacements per decay (dpa)
α-particle	~ 2×10^{-5}	3×10^{9} / 10^{10}	130 – 200
recoil nucleus	~ 3×10^{-8}	~6×10^{7} / ~3×10^{9}	120 – 2000
β-particle	~ 10^{-3}	~3×10^{9} / ~4×10^{9}	0.1 – 1
γ-radiation	~ 2×10^{-2}	~2×10^{9} / ~2×10^{9}	<<1
Spontaneous decay	~ 10^{-5}	10^3 – 10^4 ** / No data	2.5×10^4 – 5×10^5

Gray, unit of absorbed dose of radiation, Gy = J/kg; ** – for the first 100 years.

 doi:10.20944/preprints202412.0652.v1

The synthesis of actinide matrices is labour-intensive and complicated process due to the need for protection from radiation, as well as the high cost of Pu, Am, Cm isotopes. To study radiation damage, simulation techniques are typically used – irradiation with neutral or charged particles [25,26,28,50,66,68,69,85,86,93,97,99,101–111]. They allow for a very short time (minutes) to achieve radiation doses that a matrix with real HLW will accumulate over many thousands of years. The most common method for studying the radiation resistance of actinide matrices is irradiation with heavy ions. The goal of such works is to determine the critical radiation dose (D_{cr}), leading to amorphization of the structure, and the critical temperature (T_{cr}), above which amorphization does not occur at any doses. The higher the first value and the lower the second, the more resistant the phase structure is to radiation. The main advantages of irradiation with ions are: short time; no induced activity, which simplifies the study of matrices; critical doses and temperatures of all phases in the sample can be determined simultaneously; disordering is observed in an electron microscope during irradiation. Matrices are usually irradiated with 1 MeV $Kr^{+/2+}$, in which case the amorphization doses in units of displacements per atom (dpa) are close to the values during the decay of actinides [66,68,87–89,93,95,97,101].

In the REE_2O_3–ZrO_2–TiO_2 system, the phases with the pyrochlore structure have been intensely studied [66,95,97,101–105], there is a lot of data on the behaviour of REE_2TiO_5 and $REE_2Ti_2O_7$ under irradiation [69,87,97,101–111], and for $REE_4Ti_9O_{24}$ there are scarce data [111]. For the $A_2B_2O_7$ phases (A = La–Lu, B = Ti, Zr), the critical temperature decreases (the resistance to radiation increases) upon transition from REE phases with the perovskite structure to compounds with the pyrochlore structure [103–105]. We studied samples consisting of pyrochlore only (T0), as well as pyrochlore and monoclinic titanate (T15, T18, T20), orthorhombic REE titanate and rutile (IM-2, IM-9), which compositions are given in the Tables 5–7. When irradiated with 1 MeV Kr^{2+} to a dose of 25×10^{14} ion/cm^2, the structure of the zirconate phase is transformed into the fluorite lattice (Figure 8), and for the monoclinic perovskite phase, amorphization is already observed at 2.5×10^{14} ion/cm^2. This proves the resistance of zirconate pyrochlore (T0) to irradiation, zirconate-titanate pyrochlore (T15) has intermediate values of D_{cr}, low resistance is typical for monoclinic and orthorhombic rare earth titanates (Figure 9). For specific type of irradiation, T_{cr} is constant (Figure 9), and D_{cr} increases with rise of temperature, since the amorphous state is unstable. Heating leads to healing of defects, so the higher doses of irradiation are required to disorder the atoms in the lattice with increasing temperature.

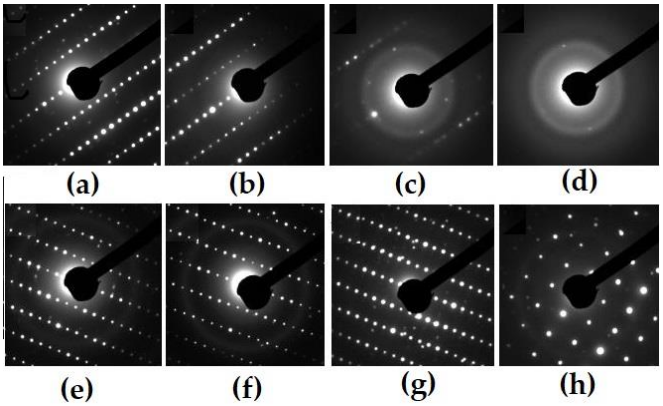

Figure 8. Electron diffraction patterns for pyrochlore (T0, a-d) and perovskite-type monoclinic REE titanate (T18, e-h) before (a, d) and after irradiation by 1 MeV Kr^{2+} to dose, 10^{14} ions/cm^2: 2 (b), 6 (c), 25 (d), 1.3 (e), 1.9 (f), 2.5 (h).

For the phase of composition $A_{1.94}Ti_{2.00}O_{6.92}$ (A is a mixture of REE as in HLW): $D_{cr} = 2.5\times10^{14}$ Kr^{2+}/cm^2, T_{cr} = 900 K. Critical doses (T = 298 K) of the phases $Nd_{3.96}(Ti_{8.92}Zr_{0.12})O_{23.94}$ and $REE_{3.95}(Ti_{8.71}Zr_{0.34})O_{24.01}$ (REE = 0.43La + 0.92Ce + 0.30Pr + 1.63Nd + 0.25Sm + 0.10Eu + 0.09Gd + 0.23Y) are determined as 3×10^{14} Kr^{2+}/cm^2 (0.2 dpa), their T_{cr} is 900 K. Similar values were obtained for

 doi:10.20944/preprints202412.0652.v1

monoclinic titanates: for $La_2Ti_2O_7$ the critical dose is defined as 2.16×10^{14} Kr^{2+}/cm^2, and the critical temperature, T_{cr} = 840 K.

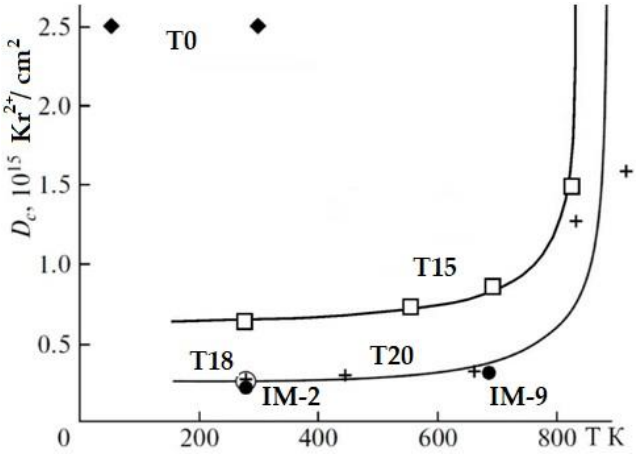

Figure 9. Amorphization doses of Ti-Zr (T15) pyrochlores, monoclinic (T18, T20) and orthorhombic (IM-2, IM-9) titanates under irradiation with 1 MeV Kr^{2+}. The structure of zirconate pyrochlore (T0) is transformed at irradiation into a defect fluorite-type lattice [97,105,111].

A sample consisting of $Nd_4(Ti,Zr)_9O_{24}$ and rutile $(Ti,Zr)O_2$ was obtained by the ICCM method [99] and irradiated with electrons beam (energy 4.5-5 MeV, beam power 20 kW, current 17 mA) to a dose of 5×10^9 Gray. Irradiation did not affect the cell parameters of the neodymium titanate and rutile phases (Figure 10), but the leaching rate of Nd and Ti from the irradiated sample with water on the 28th day increased from 10^{-5} to 10^{-4} g/($m^2\times$day).

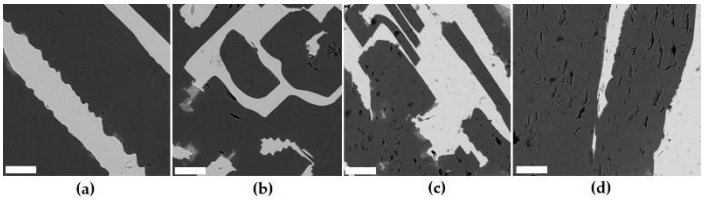

Figure 10. SEM images of the sample before (a) and after irradiation to a dose of 10^7 (b), 5×10^8 (c) or 5×10^9 Gray (d). Light is orthorhombic Nd titanate, dark is rutile. Markers are 20 micrometres.

When irradiated with 1 MeV Kr^{2+} ions, the critical temperatures of the Nd phases change from 135 and 685 K for the pyrochlores $Nd_2Zr_2O_7$ and $Nd_2Ti_{0.8}Zr_{1.2}O_7$ to 918 K for the perovskite $Nd_2Ti_2O_7$ and 1200 K for Nd_2TiO_5 [108]. At a disposal facility temperature of 300–350 K (in mines) or 400–550 K (in deep boreholes), so only pyrochlores with a Zr : Ti ratio > 1 will retain crystallinity, while the remaining compositions will be amorphized due to actinide decay. In this case, the actinide leaching rate increases by only an order of magnitude. Radiation has a direct (amorphization) and indirect (increase in acidity during radiolysis, heating) effects on the properties of actinide matrices and their behaviour in the disposal facility. The influence of amorphization on leaching is usually less than one order of magnitude. The acid pH of the solution is quickly neutralized by interaction with the container materials and the bentonite-based buffer. Temperature causes an increase in the leaching rate, but slows down the process of disordering the structure, preserving the original properties of the matrix. In general, radiation resistance is significantly less important for the selection of matrices than their corrosion resistance. Deep groundwater is represented by brines, so the leaching resistance of matrices must be studied under conditions close to these settings. Calculations were made of the thermal field of a borehole repository for the REE-actinide fraction. The estimates have considered the container diameter, waste content, and holding time before disposal [53]. Minor actinides (Am, Cm) decay will result in heating of the waste forms up to 300–500 °C for decades, while REE decay has a rather short-term effect on the matrix heating. With a waste content of 30 wt.% in the immobilising matrix, the temperature increase in 10 years will be less than 40 °C.

 doi:10.20944/preprints202412.0652.v1

8. On the Synthesis of Matrices in the REE_2O_3 (Nd_2O_3) – TiO_2 – ZrO_2 System

A material with the best properties will not become a matrix of real HLW unless it can be effectively obtained in the required volumes remotely. Given the high radiation, the availability of industrial waste forms production technology is especially important [15,28–37,39,86,112–116]. Due to its absence, the ceramics Synroc and the super-calcine proposed in the 1970s did not find practical application [25,26,28,114]. Only now, 50 years later, the technology for producing Synroc by hot pressing is close to implementation at a radiochemical plant in Australia [115]. The technologies already tested on real actinide-containing materials (waste) include melting in electric furnaces or induction crucibles, and sintering [15,37,39,86,116]. Melting has been used for over 40 years to vitrify high-level waste [25–37,112,113], sintering – for the synthesis of fuel with Pu, Np, Am – MOX, REMIX, MNUP [117–119]. Cold pressing and sintering route was developed to produce Synrocs and pyrochlore-based ceramics for weapons-based plutonium [15,26,28,39]. Hot pressing method was proposed to produce Synroc ceramics [25,114,115].

Melting methods are more preferable above the industrial technologies, as they are less sensitive to the quality of the batch and do not require the use of pressure. In the 1970s, induction melting technology was proposed for vitrification of high-level waste [25–35]. Its advantages are contactless energy supply and skull melting under active hydrodynamic conditions. In Russia, research has been conducted for over 20 years on the synthesis of induction melting in a cold crucible, ICCM of vitreous matrices and ceramics, including Synroc, zirconolite, pyrochlore, murataite, brannerite, etc. [80,81,86,99,120,121]. Abroad, the ICCM method is widely used to obtain ceramic and glass-ceramic forms with HLW simulants [28,30,39,122–125]. It allows obtaining matrices of the REE-actinide fraction at temperatures up to 2200 °C, although high temperatures require large energy costs. The REE zirconates are refractory phases, the liquidus temperatures are above 2000 °C. In titanate systems, the melting temperatures are lower: for $La_2Ti_2O_7$ and $Nd_2Ti_2O_7$, they are 1790 and 1650 °C, but for $Nd_4Ti_9O_{24}$ and the eutectic 85 mol.% $Nd_4Ti_9O_{24}$ - 15 mol.% TiO_2 they are below 1500 °C (Table 3), which makes ICCM a promising for their manufacture.

9. Discussion

Prevention of negative ecological impact of nuclear power waste is a fundamental scientific task and a practical problem. The main threat is associated with high-level waste containing long-lived actinides and fission products. Two approaches have been proposed to solve this problem: P&T (partitioning and transmutation) or P&C (partitioning and conditioning) [58,125]. The P&C approach is being developed by physicists and radiochemists; it is based on the separation of radioisotopes and their conversion into stable and short-lived isotopes upon neutron irradiation. This scheme includes the separation of HLW onto radionuclides or their groups, transmutation in a fast neutron flux, and disposal of the remaining waste. The first information on transmutation dates back to 1964 [126,127] and concerned fission products (^{90}Sr, ^{137}Cs). Transmutation of actinides in thermal water-cooled reactors (LWR), was proposed in 1972 [128], but later fast neutron reactors and subcritical installations – accelerators were chosen for this purpose as more promising [129–131]. The alternative approach (P&C) is being developed by geologists (mineralogists, geochemists), materials scientists, and some radiochemists; it involves the inclusion of waste in matrices and disposal. This method is more economical, since it requires less isotope separation and there is no need to build very complex expensive installations for deep partitioning of HLW, fuel fabrication, multiply irradiation and SNF reprocessing.

The purpose of transmutation is to reduce the environmental hazard of SNF and HLW [11,12,41,43,59,132–141] in order to achieve radiation (radioecological) equivalence of HLW and uranium ore used to manufacture nuclear fuel as quickly as possible. Calculations have shown that extraction and transmutation of 99.9% of actinides reduces this time to 100 – 300 years, which eliminates the need to construct deep geological disposal facilities. The obvious mistake of this calculations is connected with proposal on complete dissolution of HLW and uranium ore in water and the subsequent entry of radionuclides into the human body [142]. The shortcomings of the radiation equivalence concept are discussed in [143,144]. Many studies have noted the difficulties in

 doi:10.20944/preprints202412.0652.v1

implementing industrial separation of radionuclides, MA loaded fuel production, its irradiation in fast reactors, SNF reprocessing to extract actinides again [41,43,58,125,135–139,141,145–147].

For the transmutation of minor actinides, installations with accelerators [131,148–150] and molten salt reactors [151–154] are proposed. The latter do not need the actinides separation, but their problems are associated with high cost and lack of operating experience, the requirements of isotopically pure ^{7}Li and to remove fission products, high corrosive activity of the fluoride melt etc [153]. It can be assumed that the announced ambitious task of implementing large-scale transmutation in the first half of the 21st century [149] will not be realized. Due to the need for large volumes of scientific and experimental design work in the field of creating new types of reactors, fuel and materials, the use of this technology is shifted to the distant future [17]. Another problem with this approach is that in this case it will be necessary to deal with large volumes of highly active materials for many years, which creates a high risk of accidents, irradiation of personnel and the population. Therefore, the question of using transmutation comes down to the choice between risks and consequences for current (transmutation) and future (disposal of HLW) generations.

The possibility of geological isolation of actinide-containing waste is beyond doubt. There are over two thousand uranium deposits with an age of many millions of years and total resources of over 10 million tonnes [155]. Numerous data prove the absence of uranium migration in reducing environments, which determines the preservation of uranium ores as well as uranium and thorium retention in natural vitreous and crystalline materials for hundreds of millions of years [50,66,85,87,101,156]. Such environments are realized at depths of the first hundreds of meters. Arguments in favour of long-term conservation of radionuclides include the results of studies of radioactive minerals and ores, laboratory and field experiments, thermodynamic calculations and computer modelling. The world has already accumulated 30-35 thousand tonnes of vitrified HLW from the reprocessing of SNF (the main volumes are stored in France, Russia, UK, and US) [7,15,37,157], which will be placed in underground disposal facilities. In countries with an open nuclear fuel cycle without reprocessing of SNF, its geological disposal is also assumed. The protective properties of the geological environment are due to the low solubility of radionuclides in water and the high sorption capacity of rocks. This is facilitated by the slow movement of underground waters – carriers of radionuclides. A contribution to safety will be provided by sorptive bentonite buffer swelling in water, corrosion-resistant container, and durable matrix immobilising nuclear waste. Its main characteristics are high loading for waste, low leaching rate in water, and the possibility of remote fabrication on an industrial scale.

Extraction and precipitation methods are used to separate liquid HLW onto fractions [13,17,24,38,41–47,52,125,130,139,157]. In France, a pilot reprocessing of 15 kg of SNF was conducted with the separation of the REE-actinides [158]. In Russia, a plant for the separation of the Cs-Sr fraction was in operation from 1996 to 2007, and of the REE-actinides since 1999 [159]. From 1996 to 2003, 1630 m^3 of HLW were processed there and 1.73 million Curies of the REE-actinide fraction (Am, Cm) were separated by precipitation of oxalate.

During the year of operation of a LWR with a capacity of 1000 MW, 20 tonnes of SNF are formed. A plant for the reprocessing of 800 tonnes of irradiated fuel generates about 4000 m^3 of liquid HLW per year, one m^3 of such waste containing up to 90 g of Am and Cm. A fleet of reactors with a total capacity of 100 GW(e), as in the USA or Western Europe, produces up to 3 tonnes of minor actinides per year – almost equal amounts of Np and the sum of Am and Cm; the annual accumulation of the REE-actinide fraction during the reprocessing of SNF will be about 30 tonnes. In France, 350 – 400 billion kWh of electricity are produced per year at nuclear power plants [160]. This leads to an annual production of SNF containing up to 300 kg of Am and 150 kg of Cm [43], and the mass of the REE-actinide fraction will be about 10 tonnes. In 2022, Russian NPPs generated more than 220 billion kWh of electricity [161], or ~60% of that produced in France.

In the case of reprocessing of all discharged SNF and fractionation of HLW, up to 6 tonnes of REE-actinide fraction will be formed per year. Its immobilisation will require 10–20 tonnes (2–4 m^3) of matrix with 50–25 wt.% REE-actinide fraction. According to estimates, a cluster of horizontal

 doi:10.20944/preprints202412.0652.v1

boreholes drilled from a vertical wellbore, known as SuperLAT technology (Figure 11) will accommodate up to 1000 t of SNF [162] or 500 t of HLW.

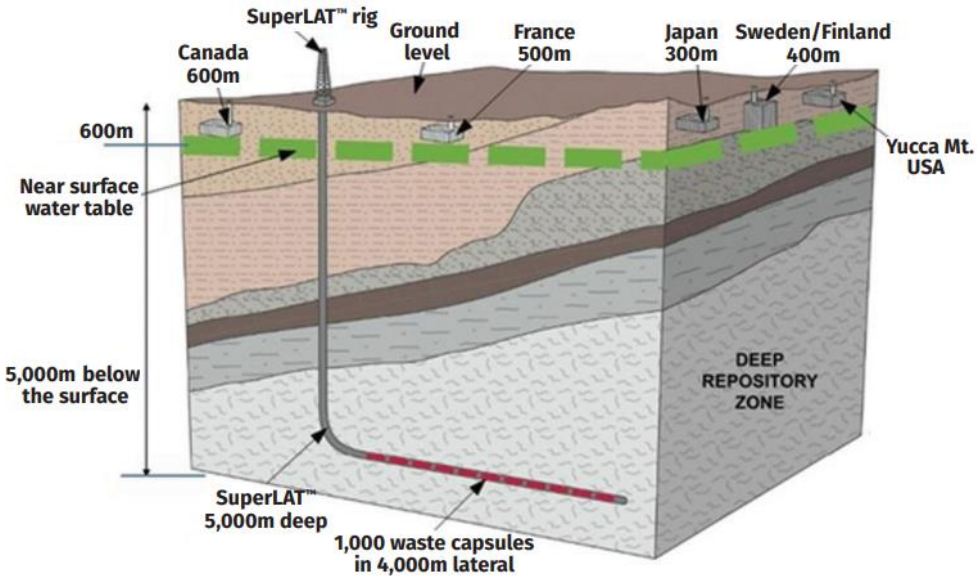

Figure 11. Horizontal wells of SuperLAT system compared to mined repositories [163].

Placing solidified actinide waste in deep disposal facilities is obviously less dangerous than injecting liquid radioactive waste (LRW), which has been practiced in Russia for about 60 years [164–166]. This technology involves injecting it into porous collectors at depths of 180 to 500 m, isolated from aquifers by clays. The total volume of LRW by 2014 exceeded 60 million m^3, the activity was 7×10^{19} Bq or ≈2 billion Curie. The actinide content in water at a distance of 100–150 m from the injection wells decreases by 10^4 – 10^6 times compared to the initial values, i.e. the bulk of the radionuclides was quickly precipitated.

The very low migration ability of actinides in underground water at reducing conditions, which are already dominant at depths of the first hundreds of meters, is evidence in favour of geological isolation of actinide wastes [125,167,168]. Programs for the geological disposal of HLW exist in many countries, including Russia [22–24,167–172]. The main contribution to human exposure will be made not by actinides, but by long-lived fission products (^{79}Se, ^{99}Tc, ^{129}I) due to their weak sorption by rocks and high migration rates in the geological environment [168,171]. Along with the traditional mine storage facilities for SNF and solidified HLW ultimate disposal [18–24,172], more and more attention is being paid to a deep boreholes – vertical, with a depth of 3 to 5 km [173–175], or initially vertical, and then horizontal at the depths of 1–3 km [162,163,176–178].

10. Concluding Remarks

Two technologies have been proposed for handling actinide-containing fractions: transmutation or immobilization. The purpose of transmutation is to reduce the amounts of long-lived radionuclides by irradiation in nuclear reactors or accelerators. The first works on this topic devoted to fission products are about 60 years old [126], 50 years ago this method was proposed for actinides [128]. Practically at the same time the study of crystalline matrices for HLW began [25]. The principles of transmutation are developed theoretically [41,137,179], and experiments on irradiation of targets with actinides have been conducted [140]. Practical implementation of the approach faces a lot of technical difficulties and high costs. Reducing the amounts of radionuclides requires multiple radiation of actinides-loaded fuel [43]. Due to increased amounts of heavy actinides, in the first turn ^{244,245}Cm [179] the irradiated targets will posses with high radioactivity, neutron fluxes and temperature, which complicates reprocessing and production of new fuel. For these purposes, fast neutron reactors are needed, in which the actinide fission dominates over neutron capture. Reasonable doubts on the benefits of minor actinides transmutation are discussed in [180]. As can be

 doi:10.20944/preprints202412.0652.v1

seen, many questions concerning the technical feasibility of effective transmutation of minor actinides, raised more than 30 years ago [181], are still relevant. Extraction and accumulation of heavy minor actinides (Am, Cm) with low (tens kg) critical masses threatens the nuclear weapons non-proliferation [182,183].

Another approach to solving the problem of long-lived radionuclides is to incorporate them into stable matrices for placement in deep geological disposal facilities. Its feasibility is demonstrated by the study of natural analogues of matrices – minerals that have retained actinides (Th,U) and REEs with properties similar to minor actinides for millions of years [50,85,87,184–186]. The presence of geological environments with a very low actinide migration is demonstrated by data on the preservation of U and Th deposits, their behaviour in the natural nuclear reactor Oklo (Gabon), studies on the solubility and sorption of actinides in laboratories and in natural (field) tests. This is supported by data on volcanic rocks confining uranium and thorium for over 140–145 million years [156].

Let us summarize the analysis of the phases of the REE_2O_3–ZrO_2–TiO_2 system as applied to the problem of REE – actinide fraction immobilisation. It is known that Nd^{3+} serves as an analogue of trivalent actinides (Am, Cm), therefore the Nd_2O_3–TiO_2–ZrO_2 system is perspective for searching hosts for REE–MA. It contains phases $Nd_2(Zr,Ti)_2O_{7-x}$, Nd_2TiO_5, $Nd_2Ti_2O_7$, $Nd_2Ti_3O_9$ and $Nd_4Ti_9O_{24}$, containing from 48 to 73 wt.% Nd_2O_3. Pyrochlore $Nd_2(Zr,Ti)_2O_{7-x}$ and titanate $Nd_4Ti_9O_{24}$ are of most interest as matrices: their stability fields (impurity content) are larger than those of other Nd titanates. With an excess of titanium, an additional phase of rutile (TiO_2) is formed, as a result of which the melting temperature decreases to 1450 – 1500 °C, which facilitates synthesis. Unlike pyrochlore, the $Nd_4Ti_9O_{24}$ compound has no analogues in nature. The content of Nd_2O_3 (actinide imitator) in it varies from 48 wt.% (only $Nd_4Ti_9O_{24}$) to 35 wt.% (70% $Nd_4Ti_9O_{24}$ and 30% rutile). Leaching rate of actinides and REE from Ti-Zr pyrochlore and REE titanates matrices in a wide range of temperatures (50–240 °C), compositions and pH of solutions (water, brines) varied in the range 10^{-3} – 10^{-5} g/(m^2 × day) and decreased with increasing interaction time. This is due to the formation of a thin surface layer enriched in zirconium and titanium, which prevents the release of REE and actinides into solution. As for the other types of matrices [187] the leaching rate in the first days is determined by their solubility, and then, due to formation of an alteration surface layer the mode changes to diffusion exchange with low velocity.

Phases of the Nd_2O_3 – TiO_2 – ZrO_2 system are considered as matrices for isolating Pu and REE-actinide fraction [62,65,68,188]. In addition to Ti-Zr pyrochlore, $Nd_4Ti_9O_{24}$ is of interest due to its higher content of impurities (Ca^{2+}, Zr^{4+}, U^{4+}) compared to Nd_2TiO_5 and $Nd_2Ti_2O_7$. With an excess of titanium, rutile (TiO_2) is formed, which reduces the melting temperature by 200–300 °C, which facilitates the synthesis of such a composite matrix.

Durable stable crystalline phases hosting long-lived radionuclides might be components of integral composite systems containing both crystalline and vitreous nuclear waste forms. There is a notable trend to use durable composite materials containing both crystalline and vitreous phases in nuclear waste immobilisation practice. The content of crystalline phases is now being increased in the glass formulations used at nuclear waste vitrification [116,189–191], which is schematically shown by the red arrow originating in the left side of the diagram (Figure 12). It is notably that the first industrial plant which uses hot pressing in Australia is now designed to synthesize composite materials with Synroc-type crystalline and mineral-like phases distributed within a glass [115,191–194].

 doi:10.20944/preprints202412.0652.v1

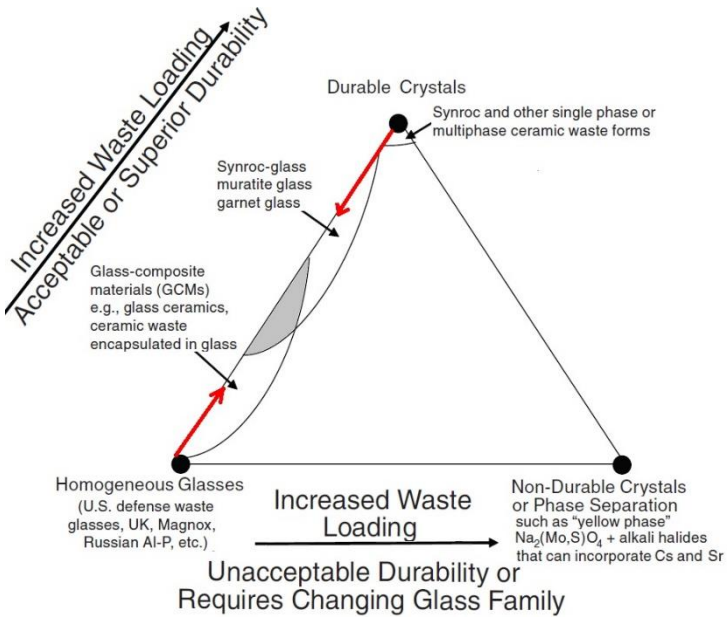

Figure 12. Composite glass-crystalline hosts for HLW are shown by the shadowed area [8,39].

Matrices of HLW are currently supposed to be placed at depths of 500–700 m in mine-type disposal facilities or in super-deep (3 to 5 km) boreholes. For the REE-actinide fraction, the borehole option is preferable; in this case, due to the increase in temperature with depth, the rocks can be heated to 200 °C and even higher values [195]. High temperature slows down the radiation destruction of the crystalline structure of actinide hosts and reduces the effect of amorphization on the leaching of radionuclides. Both the large distance to the surface and low velocity of water movement will also serve as important safety factors for the HLW disposal.

Progress in the field of methods for separating HLW [47], their incorporation into matrices [39,193] and recent achievements on geological disposal of the spent nuclear fuel and solidified high-level waste [23,195–197] allows us to expect a solution to the problem of handling the REE – minor actinides already in the coming decades. The use of transmutation for this purpose appears to be essentially more complex technological approach, required significantly more financial resources and time for implementation [17].

Author Contributions: Conception, S.V.Y.; methodology, S.V.Y. and M.I.O.; investigation, S.V.Y.; resources, S.V.Y.; sample synthesis, O.I.S.; data curation, S.V.Y., M.I.O. and O.I.S.; draft preparation, S.V.Y. and M.I.O. Authors have read and agreed to the published version of the manuscript.

Funding: The study was carried out with financial support from the Ministry of Science and Higher Education of the Russian Federation within the framework of a state assignment for the Institute of Geology of Ore Deposits, Petrography, Mineralogy and Geochemistry of the Russian Academy of Sciences. The APC was granted by MDPI.

Data Availability Statement: All data is available within the manuscript.

Acknowledgments: The authors thank M.S. Nickolsky for help in investigation of the samples.

Conflicts of Interest: The authors declare no conflict of interest.

References

1. Burnett, R.; Chen, H.; Szyszkowicz, M.; Fann, N.; Hubbell, B.; Pope, C.A.; Apte, J.S. Global estimates of mortality associated with long-term exposure to outdoor fine particulate matter. *Proceedings of the National Academy of Sciences* **2018,** *115*. 9592–9597.
2. Accelerating Decarbonization in the United States: Technology, Policy, and Societal Dimensions. The National Academies Press: Washington, DC, USA, 2024; 822p.
3. *State of Global Air 2024;* Health Effects Institute: Boston, MA, USA, 2024; 35p.

4. IEA. Net Zero Roadmap: A Global Pathway to Keep the 1.5 °C Goal in Reach 2023 Update; International Energy Agency (IEA): Paris, France, 2023; 224p.
5. IAEA. Energy, Electricity and Nuclear Power Estimates for the Period up to 2050; International Atomic Energy Agency (IAEA): Vienna, Austria, 2023; 137p.
6. NEA. Meeting Climate Change Targets. The Role of Nuclear Energy; NEA No. 7628; OECD/NEA Publishing: Paris, France, 2022; 49p.
7. IEA. *Electricity 2024. Analysis and Forecast to 2026*; International Energy Agency (IEA): Paris, France, 2024; 168p.
8. Ojovan, M.I. Vitrification as a key solution for immobilisation within nuclear waste management. *Arab. J. Sci. Eng.* **2024,** https://doi.org/10.1007/s13369-024-09292-z.
9. IEA. *World Energy Investment;* International Energy Agency (IEA): Paris, France, 2024; 215p.
10. NEA. *Transition towards a Sustainable Nuclear Fuel Cycle*; OECD/NEA Publishing: Paris, France, 2013; 67p.
11. Adamov, E.O.; Asmolov, V.G.; Bolshov, L.A.; Ivanov, V.K. Two-component nuclear power. *Bull. Russ. Acad. Sci.* **2021**, *91*, 450–458. (In Russian).
12. Adamov, E.O.; Kaplienko, A.V.; Orlov, V.V.; Smirnov, V.S.; Lopatkin, A.V.; Lemekhov, V.V.; Moiseev, A.V. BREST lead-cooled fast reactor: from concept to technological implementation. *Atomic Energy* **2021,** *129*, 179–187.
13. Kolupaev, D.N.; Apalkov, G.A. Development and tasks of radiochemical technologies: history and modern challenges. *Radiochemistry* **2023**, *65*, 132–140.
14. Holdsworth, A.F.; Eccles, H.; Sharrad, C.A.; George, K. Spent nuclear fuel—waste or resource? The potential of strategic materials recovery during recycle for sustainability and advanced waste management. *Waste* **2023**, *1*, 249–263. https://doi.org/10.3390/waste1010016.
15. Yudintsev, S.V. Isolation of separated waste of nuclear industry. *Radiochemistry* **2021**, *63*, 527–555.
16. Wang, L.; Liang, T. Ceramics for high level radioactive waste solidification. *Journal of Advanced Ceramics* **2012**, *1*, 194–203.
17. Merits and Viability of Different Nuclear Fuel Cycles and Technology Options and the Waste Aspects of Advanced Nuclear Reactors. The National Academies Press: Washington, DC, USA, 2023; 314p.
18. IAEA. Scientific and Technical Basis for the Geological Disposal of Radioactive Wastes; International Atomic Energy Agency (IAEA): Vienna, Austria, 2003; 80p.
19. *Geological Repository Systems for Safe Disposal of Spent Nuclear Fuels and Radioactive Waste*. Ahn, J.; Apted, M.J., Eds. Woodhead Publishing Limited: Cambridge, United Kingdom, 2010; 777p.
20. IAEA. *Disposal of Radioactive Waste, IAEA Safety Standards Series No. SSR-5;* International Atomic Energy Agency (IAEA): Vienna, Austria, 2011; 62 p.
21. Evans, N.D.M. Geological disposal of radioactive waste: underpinning science and technology. *Mineralogical Magazine* **2012**, *76*, 2865–2871.
22. Ewing, R.C.; Whittleston, R.A.; Yardley, B.W.D. Geological disposal of nuclear waste: a primer. *Elements* **2016**, *12*, 233–237.
23. NEA. Management and Disposal of High-Level Radioactive Waste: Global Progress and Solutions; OECD/NEA Publishing: Paris, France, 2020; 45p.
24. NEA. Strategies and Considerations for the Back End of the Fuel Cycle. OECD/NEA Publishing: Paris, France, 2021; 67p.
25. *Radioactive Waste Forms for the Future*; Lutze, W., Ewing, R.C., Eds.; Elsevier: New York, NY, USA, 1988; 778p.
26. Donald, I.W.; Metcalfe, B.L.; Taylor, R.N.J. The immobilization of high-level radioactive wastes using ceramics and glasses. *J. Mater. Sci.* **1997**, *32*, 5851–5887.
27. Caurant, D.; Loiseau, P.; Majérus, O.; Aubin-Chevaldonnet, V.; Bardez, I.; Quintas, A. *Glasses, Glass-Ceramics and Ceramics for Immobilization of Highly Radioactive Nuclear Wastes*; Nova Science Publishers: New York, NY, USA, 2009; 445p.
28. Donald, I.W. Waste Immobilisation in Glass and Ceramic Based Hosts; Wiley: Hoboken, NJ, USA, 2010; 507p.
29. Vienna, J.D. Nuclear waste vitrification in the United States: Recent developments and future options. *International Journal of Applied Glass Science* **2010**, *1*, 309–321.
30. Jantzen, C.M. Development of glass matrices for high level radioactive waste. In *Handbook of Advanced Radioactive Waste Conditioning Technologies*; Ojovan, M.I., Ed.; Woodhead Publishing Ltd: Cambridge, UK, 2011; pp. 230–292.
31. Remizov, M.B.; Kozlov, P.V.; Logunov, M.V.; Koltyshev, V.K.; Korchenkin, K.K. Conceptual and technical solutions for the creation of vitrification units for current and accumulated liquid HLW at PA Mayak. *Iss. Radiat. Saf.* **2014**, *3*, 17–25. (In Russian)
32. Vernaz, E.; Bruezière, J. History of nuclear waste glass in France. *Procedia Mater. Sci.* **2014**, *7*, 3–9.
33. Harrison, M.T. Vitrification of high-level waste in the UK. *Procedia Mater. Sci.* **2014**, *7*, 10–15.

34. Vienna, J.D.; Collins, E.D.; Crum, J.V.; Ebert, W.L.; Frank, S.M.; Garn, T.G.; Gombert, D.; Jones, R.; Jubin, R.T.; Maio, V.C.; Marra, J.C.; Matyas, J.; Nenoff, T.M.; Riley, B.J.; Sevigny, G.J.; Soelberg, N.R.; Strachan, D.M.; Thallapally, P.K.; Westsik, J.H. *Closed Fuel Cycle Waste Treatment Strategy*. Idaho National Laboratory: Idaho Falls, ID, USA, 2015; 146p.
35. Goel, A.; McCloy, J.S.; Pokorny, R.; Kruger, A.A. Challenges with vitrification of Hanford high-level waste (HLW) to borosilicate glass – An overview. *Journal of Non-Crystalline Solids: X 4* **2019**, 100033.
36. Thorpe, C.L.; Neeway, J.J.; Pearce, C.; Hand, R.J.; Fisher, A.J.; Walling, S.A.; Hyatt, N. C.; Kruger, A.A.; Schweiger, M.; Kosson, D.S.; Arendt, C.L.; Marcial, J.; Corkhill, C.L. Forty years of durability assessment of nuclear waste glass by standard methods. *npj Materials Degradation* **2021**, *61*, 5. https://doi.org/10.1038/s41529-021-00210-4.
37. Ojovan, M.I.; Yudintsev, S.V. Glass, ceramic, and glass-crystalline matrices for HLW immobilisation. *Open Ceram.* **2023**, *14*, 100355.
38. Choppin, G.; Liljenzin, J.-O.; Rydberg, J.; Ekberg, C. The Nuclear Fuel Cycle. In *Radiochemistry and Nuclear Chemistry*, 4th ed.; Elsevier: Amsterdam, The Netherlands, 2013; Chapter 21, pp. 685–751.
39. National Research Council. *Waste Forms Technology and Performance: Final Report*; National Academies Press: Washington, DC, USA, 2011; 308p. https://doi.org/10.17226/13100.
40. Petrov, V.A.; Ojovan, M.I.; Yudintsev, S.V. Material aspect of sustainable nuclear waste management. *Sustainability* **2023**, *15*, 11934. https://doi.org/10.3390/su151511934.
41. IAEA. Implications of Partitioning and Transmutation in Radioactive Waste Management; International Atomic Energy Agency (IAEA): Vienna, Austria, 2004; 126p.
42. Kopyrin, A.A.; Karelin, A.I.; Karelin, V.A. *Technology of Production and Radiochemical Processing of Nuclear Fuel*. Atomenergoizdat: Moscow, Russia, 2006; 576p. (In Russian).
43. CEA. *Treatment and recycling of spent nuclear fuel*. Commissariat à l'énergie atomique (CEA): Paris, France, 2008; 175p.
44. IAEA. *Assessment of Partitioning Processes for Transmutation of Actinides*. International Atomic Energy Agency (IAEA): Vienna, Austria, 2010; 96p.
45. NEA. *National program in chemical partitioning*. OECD/NEA Publishing: Paris, France, 2010; 119p.
46. Nash, K.L.; Madic, Ch.; Mathur, J.N.; Lacquement, J. Actinide Separation Science and Technology. In *The Chemistry of the Actinide and Transactinide Elements*; Chapter 24; Morss, L.R., Edelstein, N.M., Fuger, J., Eds.; Springer: Dordrecht, The Netherlands, 2010; Volume 4, pp. 2622–2798.
47. Baron, P.; Cornet, S.M.; Collins, E.D.; De Angelis, G.; Del Cul, G.; Fedorov, Y.; Glatz, J.P.; Ignatiev, V.; Inoue, T.; Khaperskaya, A.; et al. A review of separation processes proposed for advanced fuel cycles based on technology readiness level assessments. *Progr. Nucl. Energy* **2019**, *117*, 103091.
48. IAEA. Impact of High Burnup Uranium Oxide and Mixed Uranium-Plutonium Oxide Water Reactor Fuel on Spent Fuel Management. International Atomic Energy Agency (IAEA): Vienna, Austria, 2011; 82p.
49. Bruno, J.; Ewing, R.C. Spent nuclear fuel. *Elements* **2006**, *2*, 343–349.
50. Ewing, R.C.; Weber, W.J. Actinide *W*asteforms and *R*adiation *E*ffects. In *The Chemistry of the Actinide and Transactinide Elements*; Chapter 35; Morss, L.R., Edelstein, N.M., Fuger, J., Eds.; Springer: Dordrecht, The Netherlands, 2011; Volume 6, pp. 3813–3889.
51. Walker, C.T.; Rondinella, V.V.; Papaioannou, D.; Winckel, S.V.; Goll, W.; Manzel, R. On the oxydation state of UO_2 nuclear fuel at a burn-up of around 100 MWd / kg HM. *J. Nucl. Mater.* **2005**, *345*, 192–205.
52. Collins, E.D.; Jubin, R.T.; DelCul, G.D.; Spencer, B.B.; Renier, J.P. Advanced Fuel Cycle Treatment, Recycling, and Disposal of Nuclear Waste. In Proceedings of the International Conference "Global 2009", Paris, France, 6–11 September 2009; pp. 2595–2602.
53. Yudintsev, S.V.; Ojovan, M.I.; Malkovsky, V.I. Thermal effects and glass crystallization in composite matrices for immobilization of the rare-earth element–minor actinide fraction of high-level radioactive waste. *J. Compos. Sci*. **2024,** *8*, 70. doi:10.3390/jcs8020070.
54. Shannon, R.D. Revised effective ionic radii and systematic studies of interatomic distances in halides and chalcogenides. *Acta Cryst.* **1976**, *A32*, 751–767. https://doi.org/10.1107/S0567739476001551.
55. Troitzsch, U.; Ellis, D.J. High-PT study of solid solutions in the system ZrO_2-TiO_2: The stability of shrilankite. *Eur. J. Mineral*. **2004**, *16*, 577–584.
56. Fabrichnaya, O.; Savinykh, G.; Schreiber, G.; Seifert, H.J. Phase relations in the ZrO_2 - Nd_2O_3 - Y_2O_3 system: Experimental study and advanced thermodynamic modeling. *Journal of Phase Equilibria and Diffusion* **2011**, *32*, 284–297.
57. Gorsky, V.V. Inert mass nuclear fuel (IMF). *Nuclear Technology Abroad* **2000**, *10*, 3–8. (In Russian).
58. NEA. Potential Benefits and Impacts on Advanced Nuclear Fuel Cycles with Actinides Partitioning and Transmutation. OECD/NEA Publishing: Paris, France, 2011; 73p.
59. NEA. State-of-the-Art Report on Innovative Fuels for Advanced Nuclear System. OECD/NEA Publishing: Paris, France, 2014; 214p.
60. Gong, W.; Zhang, R. Phase relationship in the TiO_2–Nd_2O_3 pseudo-binary system. *Journal of Alloys and Compounds* **2013**, *548*, 216–221.

61. Gong, W.; Zhang, R. Thermodynamic investigation of the TiO_2–La_2O_3 pseudo-binary system. *Thermochimica Acta* **2012**, *534*, 28–32.
62. Yudintsev, S.V. Lanthanide titanates as promising matrices for immobilization of actinide wastes. *Doklady Earth Sciences* **2015**, *460*, 130–136.
63. Gong, W.; Liu, Y.; Luo, Z. Calculated Sm_2O_3 - TiO_2 phase diagram compared to experimental data. Heat capacity of samarium titanates and phase equilibria of Sm_2O_3 - TiO_2 system. *Journal of Alloys and Compounds* **2021**, *860*, 158429.
64. Yang, K.; Lei, P.; Yao, T.; Gong, B.; Wang, Y.; Li, M.; Wang, J.; Lian, J. A systematic study of lanthanide titanates ($A_2Ti_2O_7$) chemical durability: corrosion mechanisms and control parameters. *Corrosion Science* **2021**, *185*, 109394.
65. Shoup, S.S.; Bamberger, C.E.; Tyree, J.L.; Anovitz, L. Lanthanide-containing zirconotitanate solid solutions. *J. Solid-State Chem*. **1996,** *127*, 231–239.
66. Ewing, R.C.; Weber, W.J.; Lian, J. Nuclear waste disposal—Pyrochlore ($A_2B_2O_7$): Nuclear wasteform for the immobilization of plutonium and "minor" actinides. *J. Appl. Phys.* **2004**, *95*, 5949–5971.
67. Harvey, E.J.; Whittle, K.R.; Lumpkin, G.R.; Smith, R.I.; Redfern, S.A.T. Solid solubilities of (La Nd,)$_2$(Zr,Ti)$_2O_7$ phases deduced by neutron diffraction. *J. Solid State Chem*. **2005**, *178*, 800–810.
68. Laverov, N.P.; Yudintsev, S.V.; Livshits, T.S.; Stefanovsky, S.V.; Lukinykh, A.N.; Ewing, R.C. Synthetic minerals with the pyrochlore and garnet structures for immobilization of actinide-containing wastes. *Geochemistry International* **2010**, *48*, 1–14.
69. Aughterson, R.D.; Lumpkin, G.R.; Ionescu, M.; de los Reyes, M.; Gault, B.; Whittle, K.R.; Smith, K.L.; Cairney, J.M. Ion-irradiation resistance of the orthorhombic Ln_2TiO_5 (Ln = La, Pr, Nd, Sm, Eu, Gd, Tb and Dy) series. *Journal of Nuclear Materials* **2015,** *467*, 683–691.
70. Yudintsev, S.V.; Nickolsky, M.S.; Stefanovsky, O.I.; Nikonov, B.S. Crystal–chemical considerations in the choice of matrices for REE-actinides. *Doklady Earth Sciences* **2022**, *504*, 403–409.
71. Yudintsev, S.V.; Stefanovsky, S.V.; Nikonov, B.S.; Nikol'skii, M.S.; Livshits, T.S. Potential matrices for immobilization of the rare earth–actinide fraction of high-level waste in the $REE_2Zr_2O_7$ – $REE_2Ti_2O_7$ system. *Radiochemistry* **2015**, *57*, 187–199.
72. Yudintsev, S.V.; Nikolskii, M.S.; Nikonov, B.S.; Malkovskii, V.I. Matrices for isolation of actinide wastes in a deep well repository. *Dokl. Earth Sci.* **2018**, *480*, 631–636.
73. Yudintsev, S.V.; Malkovsky, V.I.; Nikolsky, M.S.; Nikonov, B.S. Interaction of actinide matrices with brine. *Dokl. Earth Sci.* **2019**, *485*, 303–307.
74. Yudintsev, S.V.; Nickolsky, M.S.; Stefanovsky, O.I.; Nikonov, B.S. Crystal chemistry of titanates and zirconates of rare earths–possible matrices for actinide isolation. *Radiochemistry* **2022**, *64*, 667–679.
75. Skapin, S.D.; Kolar, D.; Suvorov, D. Phase equilibria and solid solution relationships in the La_2O_3 – TiO_2 – ZrO_2 system. *Solid State Sciences* **1999**, *1*, 245–255.
76. Schaedler, T.A.; Fabrichnaya, O.; Levi, C.G. Phase equilibria in the TiO_2 – $YO_{1.5}$ – ZrO_2 system. *J. Eur. Ceram. Soc.* **2008**, *28*, 2509–2520.
77. Fuentes, A.F.; O'Quinn, E.C.; Montemayor, S.M.; Zhou, H.; Lang, M.; Ewing, R.C. Pyrochlore-type lanthanide titanates and zirconates: Synthesis, structural peculiarities, and properties. *Appl. Phys. Rev.* **2024**, *11*, 021337. doi: 10.1063/5.0192415.
78. Shoup, S.L.S. Synthesis and Characterization of Novel Lanthanide- and Actinide-Containing Titanates and Zircono-Titanates: Relevance to Nuclear Waste Disposal. Ph. D. Thesis. The University of Tennessee: Knoxville, USA, 1995; 131p.
79. Yudintsev, S.V.; Aleksandrova, E.V.; Livshits, T.S.; Mal'kovskii, V.I.; Bychkova, Ya.V.; Tagirov, B.R. Crystalline matrices for immobilization of actinides: corrosion resistance in water. *Doklady Earth Sciences* **2014**, *458*, 1281–1284.
80. Melnikova, I.M.; Kalenova, M.Yu.; Shchepin, A.S.; Yudintsev, S.V. Durability of matrices for the rare-earth – actinide fraction of high-level radioactive waste in water. *Doklady Earth Sciences* **2022**, *507*, S461–S467.
81. Yudintsev, S.V.; Stefanovsky, S.V.; Kalenova, M.Y.; Nikonov, B.S.; Nikolsky, M.S.; Ananyev, A.V.; Shchepin, A.S. Matrices for the immobilization of rare earth-actinide fraction waste, obtained by induction melting in a cold crucible. *Radiochemistry* **2015**, *57*, 321–333.
82. Yudintsev, S.V.; Nickolsky, M.S.; Stefanovskaya, O.I.; Nikonov, B.S.; Ulanova, A.S. Electron backscattered diffraction in the study of matrices for high-level wastes. *Doklady Earth Sciences* **2022**, *507*, 1148–1153.
83. Pilania, R.K.; Dube, C.L. Matrices for radioactive waste immobilization: a review. *Frontiers in Materials* **2023**, *10*, 1236470.
84. Stefanovsky, S.V.; Yudintsev, S.V.; Nikonov, B.S.; Mironov, A.S. Phase composition of uranium- and cerium-containing titanate and zirconate ceramics based on cubic phases with a fluorite-type structure. *Perspective Materials* **2004**, *3*, 55–62 (In Russian).
85. Lumpkin, G.R. Ceramic waste forms for actinides. *Elements* **2006**, *2*, 365–372.
86. Stefanovsky, S.V.; Yudintsev, S.V. Titanates, zirconates, aluminates and ferrites as waste forms for actinide immobilization. *Russ. Chem. Rev.* **2016**, *85*, 962–994.

87. Lumpkin, G.R. Ceramic host phases for nuclear waste remediation. In *Experimental and Theoretical Approaches to Actinide Chemistry*, 1st ed.; Gibson, J.K., de Jong, W.A., Eds.; John Wiley & Sons Ltd.: Hoboken, NJ, USA, 2018; pp. 333–377.
88. Muller, I.; Weber, W.J. Plutonium in crystalline ceramics and glasses. *Mat. Res. Soc. Bulletin* **2001**, *26*, 698–706.
89. Weber, W.J.; Navrotsky, A.; Stefanovsky, S.; Vance, E.R.; Vernaz, E. Materials science of high-level nuclear waste immobilization. *Mat. Res. Soc. Bulletin* **2009,** *34*, 46–53.
90. Kamizono, H.; Hayakawa, I.; Muraoka, S. Durability of zirconium-containing ceramic wasteforms in water. *J. Am. Ceram. Soc.* **1991,** *74*, 863-864.
91. Hayakawa, I.; Kamizono, H. Durability of a $La_2Zr_2O_7$ wasteform in water. *J. Mater. Sci.* **1993,** *28*, 513-517;
92. Yang, K.; Wang, Y.; Lei, P.; Yao, T.; Zhao, D.; Lian, J. Chemical durability and surface alteration of lanthanide zirconates ($A_2Zr_2O_7$: A = La-Yb). *Journal of the European Ceramic Society* **2021**, *41*, 6018–6028.
93. Weber, W.J.; Ewing, R.C. Radiation effects in crystalline oxide host phases for the immobilization of actinides. *Mat. Res. Soc. Symp. Proc*. **2002**, *713*, 443–454.
94. Burakov, B.E.; Ojovan, M.I.; Lee, W.E. Crystalline Materials for Actinide Immobilisation. Imperial College Press: London, United Kingdom, 2011; 197p.
95. Laverov, N.P.; Yudintsev, S.V.; Velichkin, V.I.; Lukinykh, A.N.; Tomilin, S.V.; Lizin, A.A.; Stefanovskii, S.V. Effect of amorphization on isolation properties of actinide pyrochlore matrix. Radiochemistry **2009**, *51*, 529–536.
96. Pöml, P.; Geisler, T.; Cobos-Sabaté, J.; Wiss, T.; Raison, P.E.; Schmid-Beurmann, P.; Deschanels, X.; Jégou, C.; Heimink, J.; Putnis, A. The mechanism of the hydrothermal alteration of cerium- and plutonium-doped zirconolite. *Journal of Nuclear Materials* **2011**, *410*, 10–23.
97. Yudintsev, S.V.; Lizin, A.A.; Livshits, T.S.; Stefanovsky, S.V.; Tomilin, S.V.; Ewing, R.C. Ion-beam irradiation and Cm-doping investigations of radiation damage in the crystalline nuclear waste forms for actinides. *Journal of Materials Research* **2015**, *30*, 1516–1528.
98. Shoup, S.S.; Bamberger, C.E.; Haverlock, T.J.; Peterson, J.R. Aqueous leachability of lanthanide and plutonium titanates. *Journal of Nuclear Materials* **1997**, *240*, 112–117.
99. Kuznetsov, I.V.; Zobkova, A.Yu.; Kalenova, M.Yu.; Shchepin, A.S.; Budin, O.N.; Stepanov, V.A.; Melnikova, I.M.; Stefanovskaya, O.I.; Klemazov, K.V. A study of the mechanical and thermophysical properties of crystal matrices for the immobilization of high-level wastes. *Fine Chem. Technol***. 2024,** *19*, 149–162. https://doi.org/10.32362/2410-6593-2024-19-2-149-162.
100. NEA. *Minor Actinide Burning in Thermal Reactors*; OECD/NEA Publishing: Paris, France, 2013; 78p.
101. Weber, W.J.; Ewing, R.C.; Catlow, C.R.A.; Diaz de la Rubia, T.; Hobbs, L.W.; Kinoshita, C.; Matzke, Hj.; Motta, A.T.; Nastasi, M.; Salje, E.H.K.; Vance, E.R.; Zinkle, S.J. Radiation effects in crystalline ceramics for the immobilization of high-level nuclear waste and plutonium. *J. Mater. Res.* **1998**, *13*, 1434–1484.
102. Ewing, R.C. The nuclear fuel cycle versus the carbon cycle. *The Canadian Mineralogist* **2005**, *43*, 2099–2116.
103. Lumpkin, G.R.; Pruneda, M.; Rios S. Nature of the chemical bond and prediction of radiation tolerance in pyrochlore and defect fluorite compounds. *J. of Solid State Chemistry* **2007**, *180*, 1512–1518.
104. Smith, K.L.; Blackford, M.G.; Lumpkin, G.R.; Whittle, K.; Zaluzec, N.J. Radiation tolerance of $A_2B_2O_7$ compounds at the cubic – monoclinic boundary. *Microscopy and Microanalysis* **2006**, *12*, 1094–1095.
105. Yudintsev, S.V.; Livshits, T.S.; Zhang, J.; Ewing, R.C. The behavior of rare-earth pyrochlores and perovskites under ion irradiation. *Doklady Earth Sciences* **2015**, *461*, 247–253.
106. Whittle, K.R.; Lumpkin, G.R.; Blackford, M.G. Ion-beam irradiation of lanthanum compounds in the systems $La_2O_3 – Al_2O_3$ and $La_2O_3 – TiO_2$. *Journal of Solid State Chemistry* **2010**, *183*, 2416–2420.
107. Park, S.; Lang, M.; Tracy, C.L.; Zhang, J.; Zhang, F.; Trautmann, C.; Rodriguez, M.D.; Kluthg, P.; Ewing, R.C. Response of $Gd_2Ti_2O_7$ and $La_2Ti_2O_7$ to swift-heavy ion irradiation and annealing. *Acta Materialia* **2015**, *93*, 1–11.
108. Aughterson, R.D. The Characterisation and Ion-Irradiation Tolerance of the Complex Ceramic Oxides Ln_2TiO_5 (Ln = lanthanides). Ph.D. Thesis. The University of Sydney. Centre for Microscopy and Microanalysis: Sydney, Australia. 2018; 168p.
109. Park, S.; Tracy, C.L.; Zhang, F.; Palomares, R.I.; Park, C.; Trautmann, C.; Lang, M.; Mao, W.L.; Ewing, R.C. Swift-heavy ion irradiation response and annealing behavior of A_2TiO_5 (A = Nd, Gd, and Yb). *Journal of Solid State Chemistry* **2018**, *258*, 108–116.
110. Aughterson, R. The in situ 1 MeV Kr – irradiation study of amorphisation resistance for the Ln_2TiO_5 (Ln = lanthanides and yttrium) series. A review. *Nuclear Instruments and Methods in Physics Research B* **2023**, *538*, 144–156.
111. Yudintsev, S.V. Behavior of host materials with surrogates of the rare earth–actinide fraction under ion irradiation. *Radiochemistry* **2018**, *60*, 315–321.
112. Hench, L.L.; Clark, D.E.; Campbell, J. High level waste immobilization forms. *Nucl. Chem. Waste Managem.* **1984**, *5*, 149–173.

113. Jantzen, C.M.; Ojovan, M.I. On selection of matrix (wasteform) material for higher activity nuclear waste immobilisation (Review). *Russ. J. Inorg. Chem.* **2019**, *64*, 1611–1624. https://doi.org/10.1134/S0036023619130047.
114. Ringwood, A.E.; Kesson, S.E.; Ware, N.G.; Hibberson, W.O.; Major, A. The SYNROC process: A geochemical approach to nuclear waste immobilization. *Geochemical Journal* **1979**, *13*, 141–169.
115. Gregg, D.J.; Farzana, R.; Dayal, P.; Holmes, R.; Gerry, T. Synroc technology: Perspectives and current status (Review). *J. Amer. Ceram. Soc.* **2020**, *103*, 5424–54411.
116. Ojovan, M.I.; Petrov, V.A.; Yudintsev, S.V. Glass crystalline materials as advanced nuclear wasteforms. *Sustainability* **2021**, *13*, 4117. https://doi.org/10.3390/su13084117.
117. NEA. *Fuels and Materials for Transmutation;* OECD/NEA Publishing: Paris, France, 2005; 240p.
118. Lebreton, F.; Prieur, D.; Horlait, D.; Delahaye, T.; Jankowiak, A.; Léorier, C.; Jorion, F.; Gavilan, E.; Desmoulière, F. Recent progress on minor-actinide-bearing oxide fuel fabrication at CEA Marcoule. *Journal of Nuclear Materials* **2013**, *438*, 99–107.
119. Carmack, W.J.; Braase, L.A.; Wigeland, R.A.; Todosow, M. Technology readiness levels for advanced nuclear fuels and materials development. *Nuclear Engineering and Design* **2017**, *313*, 177–184.
120. Poluektov, P.P.; Sukhanov, L.P.; Matyunin, Yu.I. Scientific approaches and technical solutions in the field of handling liquid high-level waste. *Russ. Chem. Journal* **2005**, *XLIX*, 29–41. (In Russian).
121. Stefanovsky, S.V.; Yudintsev, S.V.; Vinokurov, S.E.; Myasoedov, B.F. Chemical-technological and mineralogical-geochemical aspects of the radioactive waste management. *Geochemistry International* **2016**, 54, 1136–1156.
122. Amoroso, J.; Marra, J.C.; Tang, M.; Lin, Y.; Chen, F.; Su, D.; Brinkman, K.S. Melt processed multiphase ceramic waste forms for nuclear waste immobilization. *Journal of Nuclear Materials* **2014**, *454*, 12–21.
123. Crum, J.; Maio, V.; McCloy, J.; Scott, C.; Riley, B.; Benefiel, B.; Vienna, J.; Archibald, K.; Rodriguez, C.; Rutledge, V.; et al. Cold crucible induction melter studies for making glass ceramic wasteforms: A feasibility assessment. *J. Nucl. Mater.* **2014**, *444*, 481–492.
124. Amoroso, J.W.; Marra, J.; Dandeneau, C.S.; Brinkman, K.; Xu, Y.; Tang, M.; Maio, V.; Webb, S.M.; Chiu, W.K.S. Cold crucible induction melter test for crystalline ceramic waste form fabrication: A feasibility assessment. *Journal of Nuclear Materials* **2017**, *486*, 283–297.
125. CEA. *Nuclear waste conditioning*. Commissariat à l'énergie atomique (CEA): Paris, France, 2009; 150p.
126. Steinberg, M.; Wotzka, G.; Manowitz, B. *Neutron Burning of Long-lived Fission Products for Waste Disposal*. Technical Report BNL-8558. Brookhaven National Laboratory: Upton, New York, USA, 1964.
127. Schmidt, E. *Nuclear Transmutation of Radioactive Waste: a Review of the State of the Art*. Commission of the European Communities. Joint Research Centre: Ispra Establishment, Italy. 1985; 29p. https://www.oecd-nea.org/upload/docs/application/pdf/2020-07/neacrp-a-1988-0911.pdf.
128. Claiborne, H.C. *Neutron-induced Transmutation of High-level Radioactive Waste*. ORNL-TM-3964. Oak Ridge National Laboratory: Oak Ridge, TN, USA, 1972.
129. Foster, D.G. *Review of PNL Study on Transmutation Processing of High Level Waste*. LA-UR 74-74. Los Alamos National Laboratory: Santa Fe, New Mexico, USA, 1974.
130. National Research Council. *Nuclear Wastes: Technologies for Separations and Transmutation*. The National Academies Press: Washington, DC, USA. 1996; 592p. https://doi.org/10.17226/4912.
131. NEA. Accelerator-driven Systems (ADS) and Fast Reactors (FR) in Advanced Nuclear Fuel Cycles. A Comparative Study; OECD/NEA Publishing: Paris, France, 2020; 350p.
132. Adamov, E.O.; Mochalov, Yu.S.; Rachkov, V.I.; Khomyakov, Yu.S.; Shadrin, A.Yu.; Kashcheev, V.A. Reprocessing of spent nuclear fuel and recycling of nuclear materials in two-component nuclear power. *Atomic Energy* **2021**, *130*, 28–34.
133. Ivanov, V.K.; Chekin, S.Yu.; Lopatkin, A.V.; Menyajlo, A.N.; Maksioutov, M.A.; Tumanov, K.A.; Kashcheeva, P.V. Assessment of radiological hazard of radioactive waste using effective or organ doses: how this may affect final waste disposal. *Health Physics* **2022**, *122*, 402–408.
134. Ivanov, V.K.; Lopatkin, A.V.; Spirin, E.V.; Solomatin, V.M. Radiation (radiological) equivalence of radioactive waste and natural uranium raw materials: technology for ensuring the safety of current and future generations. *Nuclear and radiation safety* **2023**, *2*, 31–41. (In Russian)
135. Konings, R.J.M.; Kloosterman, J.L. A view of strategies for transmutation of actinides. *Progress in Nuclear Energy* **2001,** *38*, 331–334.
136. Berthou, V.; Degueldre, C.; Magill, J. Transmutation characteristics in thermal and fast spectra: application to americium. *Journal of Nuclear Materials* **2003**, *320*, 152-162.
137. NEA. Physics and Safety of Transmutation Systems. A Status Report; OECD/NEA Publishing: Paris, France, 2006; 120p.
138. Westlen, D. Reducing radiotoxicity in the long run. *Progress in Nuclear Energy* **2007**, *49*, 597–605.
139. Salvatores, M.; Palmiotti, G. Radioactive waste partitioning and transmutation within advanced fuel cycles: Achievements and challenges. *Progress in Particle and Nuclear Physics* **2011**, *66*, 144-166.

140. Nakajima, K., Ed. Nuclear Back-end and Transmutation Technology for Waste Disposal. Beyond the Fukushima Accident. Springer, 2015; 341p. DOI 10.1007/978-4-431-55111-9.
141. Sun, X.Y.; Han, L.H.; Li, X.X.; Hu, B.L.; Luo, W.; Liu, L. Transmutation of MAs and LLFPs with a lead-cooled fast reactor. *Scientific Reports* **2023**, *13*, 1693.
142. Ojovan, M.I.; Lee, W.E.; Kalmykov, S.N., Eds. *An Introduction to Nuclear Waste Immobilisation*, 3rd ed.; Elsevier: Amsterdam, The Netherlands, 2019; 497p.
143. Kudryavtsev, E.G.; Sharafutdinov, R.B.; Kuryndin, A.V.; Shapovalov, A.S. On the issue of achievability of radiation (radiological) equivalence of radioactive waste and natural uranium. *Nuclear and radiation safety* **2022**, *4*, 73–83. (In Russian).
144. Linge, I.I.; Utkin, S.S. Deep disposal of radioactive waste in the context of the radioequivalent approach. *Nuclear and radiation safety* **2023**, *2*, 42–56. (In Russian).
145. Korobeynikov, V.V.; Kolesov, V.V.; Karazhelevskaya, Yu.E.; Terekhova, A.M. Studies of the possibility of americium burning and transmutation in a reactor with Am-fuel. *Bulletin of Universities. Nuclear Power Engineering* **2019**, *2*, 153–163. (In Russian).
146. Korobeynikov, V.V.; Kolesov, V.V.; Ignatiev, I.A. Calculation modeling of minor actinide burning in a BN-600-type reactor with fuel without uranium and plutonium. *Bulletin of Universities. Nuclear Power Engineering* **2022**, *3*, 134–145. (In Russian).
147. Dekusar, V.M.; Moseev, A.L.; Gurskaya, O.S. *Forecast of Minor Actinide Production in the 21st Century*. Joint Scientific Centre "RF – IPPE": Obninsk, Russia, 2023; 17p. (In Russian).
148. Seltborg, P. *Source Efficiency and High-energy Neutronics in Accelerator-driven Systems*. Doctoral Thesis. Department of Nuclear and Reactor Physics Royal Institute of Technology: Stockholm, Sweden, 2005; 223p.
149. NEA. A European Roadmap for Developing Accelerator Driven Systems for Nuclear Waste Incineration; OECD/NEA Publishing: Paris, France, 2001; 145p.
150. Bevelacqua, J.J. Speculative high-level nuclear waste processing methods. *Qeios* **2023.** www.qeios.com/read/ERXS1B.
151. Ignatiev, V.; Feynberg, O.; Gnidoi, I.; Merzlyakov, A.; Surenkov, A.; Uglov, V.; Zagnitko, A.; Subbotin, V.; Sannikov, I.; Toropov, A.; Afonichkin, V.; Bovet, A.; Khokhlov, V.; Shishkin, V.; Kormilitsyn, M.; Lizin, A.; Osipenko, A. Molten salt actinide recycler and transforming system without and with Th–U support: Fuel cycle flexibility and key material properties. *Annals of Nuclear Energy* **2014**, *64*, 408–420.
152. Serp, J.; Allibert, M.; Benes, O.; Delpech, S.; Feynberg, O.; Ghetta, V.; Heuer, D.; Holcomb, D.; Ignatiev, V.; Kloostermang, J.L.; Luzzi, L.; Merle-Lucotte, E.; Uhlír, J.; Yoshioka, R.; Zhimin, D. The molten salt reactor (MSR) in generation IV: Overview and perspectives. *Progress in Nuclear Energy* **2014**, *77*, 308–319.
153. IAEA. *Status of Molten Salt Reactor Technology*. International Atomic Energy Agency: Vienna, Austria, 2023; 315p.
154. Westlén, D. *Why Faster is Better – On Minor Actinide Transmutation in Hard Neutron Spectra*. Doctoral Thesis. School of Engineering Sciences: Stockholm, Sweden, 2007; 144p.
155. NEA. *Uranium 2022: Resources, Production and Demand;* OECD/NEA Publishing: Paris, France, 2023; 561p.
156. Poluektov, V.V.; Petrov, V.A.; Ojovan, M.I.; Yudintsev, S.V. Uranium retention in silica-rich natural glasses: nuclear waste disposal aspect. *Ceramics* **2023**, *6*, 1152-1163. https://doi.org/10.3390/ceramics6020069.
157. IAEA. *Status and Trends in Spent Fuel and Radioactive Waste Management*. International Atomic Energy Agency (IAEA): Vienna, Austria. 2022; 88p.
158. Poinssot, C.; Rostaing, C.; Baron, P. Main results of the French program on partitioning of minor actinides, a significant improvement towards nuclear waste reduction. *Procedia Chemistry* **2012**, *7*, 358–366.
159. Logunov, M.V.; Voroshilov, Yu.A.; Babain, V.A.; Skobtsov, A.S. Experience in development, industrial operation and optimization of complex extraction-precipitation technology for fractionation of liquid high-level waste at the Mayak Production Association. *Radiochemistry* **2020**, *62*, 700–722.
160. WNA. *World Nuclear Performance Report 2024*. World Nuclear Association, 2024; 60p.
161. *Results of the Activities of the Electric Power Division of the State Corporation "Rosatom"*. Moscow, Russia. 2022; 46p. https://report.rosatom.ru/go/2022/rea_2022.pdf. (In Russian).
162. Crichlow, H. Solving the Nuclear Waste Problem in 2021 – A New Deep Geological Waste Repository System. 2021; 32p. www.researchgate.net.publication.3570569.
163. Crichlow, H. Looking very deep for disposal. *Nuclear Engineering International* **2023**, 40–43. www.neimagazine.com.
164. Rybalchenko, A.I.; Kurochkin, V.M.; Ershov, B.G.; Zakharova, E.V.; Kosareva, I.M.; Zubkov, A.A. 50 years of deep disposal of liquid radioactive waste – practical and scientific results. *Geoecology* **2014,** 1, 86–90. (In Russian).
165. Ershov, B.G.; Gordeev, A.V.; Kosareva, I.M. Modern problems of safe disposal of liquid radioactive waste in geological formations: radiation-chemical transformations and gas formation. *Radiochemistry* **2014**, *56*, 545–553.

166. Glinskii, M.L.; Pozdniakov, S.P.; Chertkov, L.G.; Zubkov, A.A.; Danilov, V.V.; Bakshevskaia, V.A.; Samartsev, V.N. Regional flow and transport simulation of liquid radioactive waste disposal at the siberian chemical combine for long- and super-long-term postinjection periods. *Radiochemistry* **2014**, *56*, 649–656.
167. Tsebakovskaya, N.S.; Utkin, S.S.; Kapyrin, I.V.; Medyancev, N.V.; Shamina, A.V. *Review of Foreign Practices of SNF and RW Disposal*. Komtekhprint Publishing House: Moscow, Russia. 2015; 208p. (In Russian).
168. Abalkina, I.L.; Bolshov, L.A.; Kapyrin, I.V.; Linge, I.I.; Savelyeva, E.A.; Svitelman, V.S.; Utkin, S.S. *Justification of Long-term Safety of SNF and RW Disposal for 10,000 Years or More: Methodology and Current State.* IBRAE RAS: Moscow, Russia. 2019; 40p. (In Russian).
169. Arentsen, M.; Van Est, R., Eds. The Future of Radioactive Waste Governance. Lessons from Europe. Springer, 2023; 345p.
170. Kochkin, B.T.; Linge, I.I., Eds. Disposal of Radioactive Waste at the Yeniseisky Site in Krasnoyarsk Krai: History of Site Selection and Current State of Research. Nauka: Moscow, Russia. 2024, 368p. (In Russian).
171. NEA. The Safety Case for Deep Geological Disposal of Radioactive Waste: 2013 State of the Art; OECD/NEA Publishing: Paris, France, 2014; 450p.
172. El-Showk, S. Final resting place. *Science* **2022**, *375*, 806–810.
173. Ringwood, A. Disposal of high-level nuclear wastes: A geological perspective. *Mineral. Mag.* **1985**, *49*, 159–176.
174. Gibb, F.G.G. A new scheme for the very deep geological disposal of high-level radioactive waste. *J. Geol. Soc. Lond.* **2000,** *157*, 27–36.
175. Beswick, A.J.; Gibb, F.G.F.; Travis, K.P. Deep borehole disposal of nuclear waste: Engineering challenges. *Proc. Inst. Civil Eng. Energy*. **2014**, *167*, 47–66.
176. Crichlow, H. Method of disposing of nuclear waste in underground rock formations. United States Patent US 5,850,614. 1998.
177. Crichlow, H. Method for temporary or permanent disposal of nuclear waste using multilateral and horizontal boreholes in deep isolated geologic basins. United States Patent US 6,238,138. 2001.
178. Muller, R.A.; Finsterle, S.; Grimsich, J.; Baltzer, R.; Muller, E.A.; Rector, J.W.; Payer, J.; Apps, J. Disposal of high-level nuclear waste in deep horizontal drillholes. *Energies* **2019**, *12,* 2052.
179. Sun, X.Y.; Han, L. H.; Li, X.X.; Hu, B.L.; Luo, W.; Liu, L. Transmutation of MAs and LLFPs with a lead-cooled fast reactor. *Scientific Reports* **2023**, *13*. 1693.
180. Frieß, F.; Liebert, W. Inert-matrix fuel for transmutation: Selected mid- and long-term effects on reprocessing, fuel fabrication and inventory sent to final disposal. *Progress in Nuclear Energy* **2022**, *145*, 104106.
181. Baetsle, L.H. Burning of actinides: A complementary waste management option? *IAEA Bulletin* **1992**, *3*, 32–34.
182. Westfall, R. M. Critical masses for the even-neutron-numbered transuranium actinides. *Nuclear Science and Engineering* **1981,** *79*, 237–239. DOI: 10.13182/NSE81-4.
183. Korobeynikov, V.V.; Kolesov, V.V.; Ignatiev, I.A. Computational simulation of minor actinide burning in a BN-600 reactor with fuel without uranium and plutonium. *Nuclear Energy and Technology* **2023**, *9*, 59–64. https://doi.org/10.3897/nucet.9.102776.
184. Lumpkin, G.R. Alplha-decay damage and aqueous durability of actinide host phases in natural systems. *Journal of Nuclear Materials* **2001**, *289*, 136–166.
185. Omel'yanenko, B.I.; Livshits, T.S.; Yudintsev, S.V.; Nikonov, B.S. Natural and artificial minerals as matrices for immobilization of actinides. *Geol. Ore Depos.* **2007**, *49*, 173–193.
186. Lumpkin, G.R.; Gao, Y.; Giere, R. The role of Th-U minerals in assessing the performance of nuclear waste forms. *Mineralogical Magazine* **2014**, *78*, 1071–1095.
187. Zhang, S.; Teng, Z.; Wu, L.; Tan, Y.; Chen, C.; Zhou, X. Chemical stability and leaching mechanism of YIG and HEG at different pH conditions. *J. Am. Ceram. Soc.* **2024**, *107*, 7352–7363.
188. Aughterson, R.D.; Lumpkin, G.R.; Smith, K.L.; Cairney, J.M. Novel complex ceramic oxides, Nd_2TiO_5 (Nd = La, Sm, Gd, Tb, Dy, Ho, Er, and Yb), for polyphase nuclear waste-forms. *J. Am. Ceram. Soc.* **2020**, *103,* 5536–5545.
189. Gribble, N.R.; Short, R.; Turner, E.; Riley, A.D. The impact of increased waste loading on vitrified HLW quality and durability. *Mat. Res. Soc. Symp. Proc*. **2009**, *1193*, 283.
190. Gribble, N.R.; Short, R.; Dunnett, B.; Steele, C.J. Increased molybdenum loading for vitrified high level waste. *Mat. Res. Soc. Symp. Proc.* **2014**, *1665*, DOI: 10.1557/opl.2014.652.
191. McCloy, J.S.; Schuller, S. Vitrification of wastes: From unwanted to controlled crystallization, a review. *Comptes Rendus. Géoscience* **2022**, *354* (Suppl. S1), 121–160. https://doi.org/10.5802/crgeos.111.
192. Gregg, D. Industrialization of hot isostatic pressing for the treatment of ANSTOs intermediate level liquid waste. IAEA Technical Meeting on High Temperature Processing of Radioactive Waste, IAEA, Vienna, Austria, 2 – 16 August 2024.

193. Zhang, Y.; Kong, L.; Ionescu, M.; Gregg, D.J. Current advances on titanate glass-ceramic composite materials as waste forms for actinide immobilization: A technical review. *J. European Ceramic Society* **2021,** *42*, 1852–1876. https://doi.org/10.1016/j.jeurceramsoc.2021.12.077.
194. McCloy, J.S.; Riley, B.J.; Dixon Wilkins, M.C.; Evarts, J.S.; Bussey, J.; Vienna, J.D.; Bingham, P.A.; Gregg, D.J.; Ojovan, M.; Schuller, S.; Uruga, K.; Perret, D.; Regnier, E.; Giboire, I.; Umb, W.; Xu, K.; Goel, A.; Kruger, A.A. International perspectives on glass waste form development for low-level and intermediate-level radioactive waste. *Materials Today* **2024**, xxx, xx, xx-xx. https://doi.org/10.1016/j.mattod.2024.08.025
195. Brady, P.V.; Freeze, G.A.; Kuhlman, K.L.; Hardin, E.L.; Sassani, D.C.; MacKinnon, R.J. Deep borehole disposal of nuclear waste: US perspective. In *Geological Repository Systems for Safe Disposal of Spent Nuclear Fuels and Radioactive Waste*, 2nd ed.; Apted, M., Ahn, J., Eds.; Woodhead Publishing Series in Energy: Sawston, UK, 2017; Chapter 4, pp. 89–112.
196. IAEA. *Radioactive Waste Management. Solutions for a Sustainable Future*. Proc. of an International Conference. Vienna, Austria, 1-5 November 2021. International Atomic Energy Agency (IAEA): Vienna, Austria. 2023; 475p.
197. IAEA. *Roadmap for Implementing a Geological Disposal Programme.* International Atomic Energy Agency. IAEA: Vienna, 2024; 83p.